EVALUATION AND ELIMINATION OF DEFECTS IN GLASS TO METAL SEALING USED IN AEROSPACE APPLICATIONS

MS THESIS

SYED ARIF ALI SHAH KAKAKHEL
(2006-NUST-MS-MSE-07)

SUPERVISOR
Dr. AMIR AZAM KHAN

CO-SUPERVISOR
DR. FIAZ AHMED

SUBMITTED IN PARTIAL FULFILLMENT OF THE REQUIREMENT OF

DEGREE OF MASTERS OF SCIENCE

IN MATERIAL & SURFACE ENGINEERING

SCHOOL OF CHEMICAL AND MATERIAL ENGINEERING

NATIONAL UNIVERSITY OF SCIENCE AND TECHNOLOGY, ISLAMABAD

ABSTRACT

Glass-to-metal seals are used in a variety of applications specifically in the field of medical, military, consumer products, aerospace and aviation etc. These seals are composed of various alloying metals and different combination of glass powders such as a low silica glass powder with stainless steel 304 or a borosilicate glass with Titanium, Molybdenum or Kovar alloy (54%Fe, 29%Ni, 17% Co). In our study, the microstructural basis of the bonding of borosilicate glass with Kovar alloy joints has been investigated where the Kovar alloy was pre-oxidized at 750°C for 10min in air. Glass beads were prepared from two different types of glass powders having almost closer true density and matching thermal coefficient of expansion (CTE). The green compact of glass beads was pre-sintered at 150°C for 60min followed by burn out of paraffin at 450°C for 60min. Pores were observed in the glass beads by SEM investigation which are beneficial in the glass-metal seals. The glass was bonded to the alloy by melting at 925 °C keeping different speeds of the moving belt in the belt furnace in a controlled N_2 environment by purging N_2 gas at different rates.

The effects of various process parameters studied by scanning electron microscopy revealed that a belt speed of 3cm/min and purging N_2 gas at 5m^3/hr in the furnace resulted in a defected glass-metal seal. Keeping lower belt speed at 2.5cm/min by allowing more time to the glass-to–metal joint to form under the N_2 environment at 6m^3/hr were the optimum conditions for gaining a hermetic glass-metal seal. The SEM of the different specimens revealed an iron oxide (FeO) interlayer in the joint formed under these conditions. The controlled thickness of FeO layer improves the hermeticity between the glass powder and the Kovar alloy.

ACKNOWLEDGEMENTS

My sincere appreciations to Mr Khalid Akbar, (SCME) and Mr. Mohammad Yousuf (NDC) for their technical support in showing how to perform critical task (experiments etc.) so as to complete this research. On this note, I would like to mention fellow graduate students who offered a helping hand in time of need.

How can I forget the assistance of SCME Staff who always helped me whenever I needed?

I also acknowledge the role of SCME NUST for providing me the funding for this project.

At last, I thank to my mother and wife who supported and enhanced my courage all the time to get spare myself for completing this MS program for which they sacrificed lot of their moments and occasions.

TABLE OF CONTENTS

Page No

List of Figures

Figure No **Page No**

Figure No **Page No**

List of Tables

CHAPTER 1

INTRODUCTION

1.1 Glass-to-Metal Seal

This study is intended to serve as an over view of key issues related to serve the needs of advanced battery technologies through the use of glass-to-metal seals. Many lithium and non-lithium systems (zinc-silver oxide, nickel-cadmium, thermal systems etc) offer higher energy densities, longer shelf lives, and improved operating characteristics over traditional chemistries used in battery systems. These battery systems require advanced methods of sealing e.g. hermetic glass-metal seals are required for reliable performance in a variety of applications.

As all markets and technologies face the realities of change, the battery marketplace is no different. New, more sophisticated battery chemistries have opened avenues of opportunity for firms with a keen focus on specific market needs; whether military, medical, industrial, or consumer- related.

Lithium battery systems are one of the newer technologies that are fundamentally changing user expectations and demands for increased battery performance characteristics. For instance: prior to the development of lithium batteries, heart pacemakers were powered by batteries that offered, typically, two years of service. The inconvenience associated with replacing these batteries is obvious. Lithium iodine systems offer a useful service life of approximately 10 years, while providing additional functions for the user. These increased capabilities are a tremendous benefit to the pacemaker patients, the true "users" of these products[1].

1.1.1 Lithium Battery Systems

The batteries with weld able feed-through especially hermetically sealed lithium batteries have glass to metal seals with organic electrolytes containing lithium salts which are intended for long term use in implantable medical devices and aerospace applications.

1.1.2 Zinc-Silver Oxide Battery Systems

The zinc-silver oxide batteries are electrochemical systems having primary (non-rechargeable) or secondary (rechargeable) types that use electrolyte such as KOH for their longer operating periods. These systems are provided with glass to metal seals that are corrosion resistant to the electrolytes or other environmental effects.

1.1.3 Thermal Battery Systems

Thermal battery systems that are one-shot electrochemical power sources and remain inert until an internal charge of pyrotechnic is ignited, to melt and render conductive the normally solid electrolyte, also use the glass to metal seals and provide hermeticity to the batteries to be used for long term applications in specifically in aerospace. The electrochemical systems of thermal batteries earlier were Ca/LiCl: KCl/CaCrO$_4$ or Mg/LiCl: KCl/V$_2$O$_5$, but these systems had severe disadvantages, mainly due to unwanted chemical side reactions when the battery was active. Calcium and magnesium have now been replaced with lithium or lithium alloy as the anode material with FeS$_2$ as the active cathode.

These systems can discharge at high current densities-upto several A/cm^2. At current densities of a few hundred mA/cm^2, the cell potential is about 1.6 V. These batteries have hygroscopic nature, so these are made under extreme dry conditions and sealed with metallic containers. A wide range of these batteries have different electrical

outputs that can vary from a watt for ten milliseconds, to several kW for ten minutes or more. Some high power outputs of lithium thermal batteries are shown in figure 1.1. Lithium thermal battery offers the major advantages of ruggedness, inertness, robustness, and reliability during storage (electrolyte solid and non-conducting, hermetically sealed assembly) and ability to operate over a wide temperature between 450 °C to 550 °C with a limited active life (from seconds i.e.<10s to tens of minutes according to battery size and internal construction).

Figure 1.1: Some typical high power lithium thermal batteries in which hermetic glass to metal sealing is employed. The four output terminals made of Kovar bonded with glass seals can be seen. (Courtesy: National batteries Pvt. Ltd. Pakistan)

The thermal battery is so well-suited to its application that in the smaller sizes, it is difficult to postulate an alternative. They do not need to be replaced during the life a flight of plane or space shuttle. Larger batteries, generating upto several kW for ten minutes or more are the best competitors with the equivalent reserve type silver-zinc battery.

Low silica glasses such as Ta-23 glass were developed for glass to metal seals for hermetically sealed batteries with lithium containing electrolyte composition. They are

highly resistant to lithium ion attack for long term battery applications (typically 7 to 10 years) and are highly effective insulators.

In the hermetically sealed feed-through, a feed-through pin bonded to the center of the glass seal is typically Mo and/ or Kovar due to its resistance to the corrosive effects of battery materials and its close match with the thermal coefficient of expansion characteristics of the glass. However, molybdenum also has a serious disadvantage in that it is difficult to make reliable electrical connections by welding to the Mo pin. Molybdenum can react with the atmospheric moisture to form an oxide layer which can resist effective welding. The low ductility property of Mo also makes its welding difficult[2]. So the best choice for hermetic glass seals is the Kovar, in which welding can be avoided i.e. the sealed joint is achieved by melting the glass completely to form a joint between the Kovar pin and body of the battery container.

1.2   Construction of Glass-to-Metal Seal

In construction, the glass to metal seals requires a hermetic /non-hermetic seal between the glass and the metal usually having the close-matched coefficient of thermal expansion to each other. In the simplest case, as shown in fig (1.2), a seal consists of an inner metal pin, an insulating glass collar, and an outer metal shell. To remain hermetic for the life of the component, a seal must exhibit two characteristics: strong chemical bonds at the glass-metal interfaces, and low residual tensile stresses in the glass. Interfacial chemical bonds are usually formed by pre-oxidizing the metal surfaces to ease the transition from ionic/covalent oxide bonding in the glass to metallic bonding in the pin and shell. Residual stresses are generated because metals and glasses contract at

different rates when cooled from the sealing temperature (above the softening point of the glass).

The glass-to-metal sealing–joining technology is mainly applied to power sources used in aviation structures, which requires relatively high reliability and durability. Microelectronic mechanical system (MEMS) devices and package structures are another main usage of the glass-to-metal sealing. The microfluidic joints consisting of Kovar metal tubes and silicon using borosilicate glass for high pressure are main concern. The gap between individual metallic components and the external environment have to be properly and tightly sealed in order to achieve ideal isolation, good heat insulation and quality optical properties.
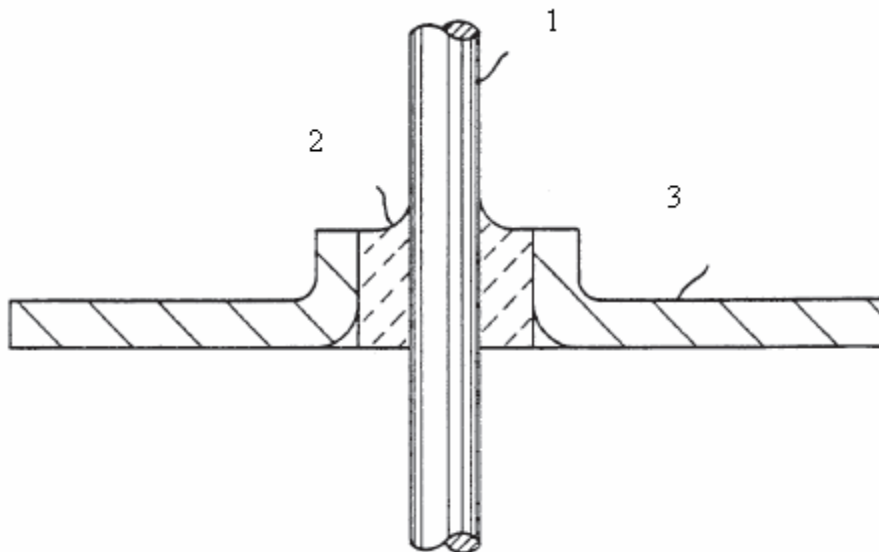
Figure 1.2: Sectional view of glass-to-metal seal. (1) Electrical lead pin, (2) insulating glass, (3) lid of the container

In sealing and joining of microelectronic packages, glass serves as an important raw material because it can be easily shaped into different dimensions as required for bonding with metal [3,4,5,6,7].

Kovar alloy (ASTM F-15), cold-rolled steel, Copper (Cu), Tantalum (Ta), Titanium (Ti) and Molybdenum (Mo) are the most commonly used metals in glass-metal seals. To get quality sealing, we have to pay attention to the heat conductivity, heat expansibility, mechanical properties and chemical stability of the metal to be employed [8,9].

Kovar-borosilicate glass seals are frequently employed in electronic and vacuum applications that are mainly used in aerospace and medical fields. The materials exhibit excellent thermal expansion match, good wettability and bond strength.[10] In addition to the close-matched thermal expansion coefficient, thermal conductivity is another important property that decides and controls the cooling rate. In certain instances, attention is paid on the mechanical and other physical properties like density etc.

In most cases, Kovar alloy is chosen due to considerations of reliability and cost. However, there exist problems of poor adherence between glass and metal, resulting in weak bonding and low-quality junction that can be improved by adopting different measures. Glass-to-metal adherence involves the wetting of glass on the metal surface and the subsequent chemical reactions and mechanical bonding [11,12,13,14]. Generally, the wettability is assessed by the contact angle. A glass-to-metal contact angle of less than 90◦ indicates good wetting; while that exceeding 90◦ implies poor wettability. A small contact angle would mean less surface tension. In terms of surface energy, better wettability is attained with smaller surface energy [2,3,15,16,17].

Reaction at the interface between glass and Kovar alloy becomes a driving force ($\gamma_{sv} - \gamma_{sl}$) behind wetting. Strong reaction, with driving force exceeding γ_{lv} triggers the wetting phenomenon. The spreading of the melted glass will stop when the reaction is completed. Moderate reaction, achieves a small contact angle of less than 90∘, indicating fair wetting, with interface energy in the order of $\gamma_{sv} > \gamma_{sl} > \gamma_{lv}$. In the absence of any reaction at the interface, the contact angle will become much bigger. Contact angle exceeding 90° signifies poor wetting, with interface energy in the order of $\gamma_{sv} < \gamma_{sl} < \gamma_{lv}$. Results of the wetting experiments would offer explanation for and information of the solid-state reactions occurring at the interface. These reactions that involve changes in the state of elements at the interface provide the driving force ($\gamma_{sv} - \gamma_{sl}$) behind wetting. When this driving force exceeds the energy at the glass surface, spreading of the melted glass will occur. Wetting at the interface indicates adhesion of glass to the alloy surface, which will facilitate sealing and joining.

It is essential for a glass to metal seal, to do pre-oxidation of the metal, which produces a thin superficial oxide layer. This oxide layer reacts subsequently with glass to make a strong junction between glass and metal. This bonding thermal treatment is achieved at temperatures near to that of glass softening, and during cooling the difference in thermal expansion between glass and metal may generate interfacial strains strong enough to break the junction. To prevent this, special alloys and glasses are used, having similar thermal expansion.

To understand the need for glass-to-metal seals in battery applications, it can best be described by classifying the battery chemistries according to the nature of the cathode

or electrolyte material. The four classifications are: solid cathodes, soluble cathodes, liquid electrolytes, and solid electrolytes.

1.2.1 Solid Cathodes

These cathode materials are typically oxides or halides. Batteries of this design do not generally require a glass-to-metal hermetic seal since the cells do not operate under pressure of the reactant materials.

1.2.2 Solid Electrolytes

These chemistries may be organic or inorganic by nature. A common solid electrolyte system is lithium iodine, used principally within medical heart pacemaker applications because of its long shelf and service life. Glass-to-metal seals are commonly found in these applications in order to provide an extremely high level of reliability and integrity.

1.2.3 Soluble Cathodes/ Liquid Electrolytes

The reaction of these materials, typically liquids or gases, often causes the battery cell to remain under pressure. Because of the pressure built up within the cell, hermetic glass-to-metal seals have found widespread use in batteries of these types.

Glass-Metal seals are a reliable method of making a long-life seal capable of operating under a wide range of conditions. These seals are capable of withstanding extremes of temperature, electrical current, pressure variations, and corrosive chemicals.

Simplistically, a glass-to-metal seal assembly consists of concentric rings of glass and metal which electrically isolate a central conductor terminal or pin from the terminal assembly body. The body is designed so that it will hermetically/ non-hermetically seal

off a container when it is welded in place, there by ensuring integrity and reliability of the seal over time.

Basically, the manufacturing consists of processing the three components (the conducting terminal or pin, the glass and the body) into a final seal assembly. The specially formulated glass is crushed, powdered and then pressed or drawn into precisely shaped glass tubing. The metal components and glass tubing are held in position by a graphite fixture while the glass softens and fuses to the metal in a controlled atmosphere oven.

Because of the large temperature difference between the furnace sealing temperatures and ambient, the thermal expansion relationship between the metals and glass is the primary consideration in designing a seal assembly.

With the various environments that glass-to-metal seals are used in, these are designed specifically for the application to meet a wide range of unique requirements; whether temperature, electrical current, pressure, or corrosive.

Two types of glass-to-metal seals can be designed: Compression seals, and Matched seals, to limit residual tension in the glass. In matched seals, the glass contraction is tailored to resemble that of the metal; and in unmatched (compression) seals, the glass is put into compression by a metal shell with a higher expansion coefficient. The latter class is used to seal a high expansion metal shell such as stainless steel 304 to a relatively low expansion silicate glass in a coaxial geometry with a pin whose expansion coefficient matches to that of the glass. To make compression seals, the seal geometry and material both are restricted[18]. In this case a close matches of thermal

expansion coefficient of the two mating bodies i.e. the glass and the alloy (mostly Kovar) is required.

The combinations of metals most commonly found in battery applications as eyelets, lids, and pins dictates that virtually all glass-to-metal seals for lithium batteries are of the compression type. A compression seal may also be made by purposely mismatching the thermal expansions of the various materials so that the highest thermal expansion metal surrounds the glass which, in turn, surrounds the similar or lower thermal expansion metal pin. Consequently, as the assembly is cooled from the glass fusion temperature, the higher thermal expansion materials contract around the lower expansion materials with a large net compressive stress exerted between the pin and the metal body. Hermeticity is achieved through the compression fit between the components.

The compression seal takes advantage of the high tensile strength of metals and high compressive strength of glass. Because glass fracture toughness is low (for certain glasses), residual tensile stress in the glass (and the resulting stress intensity factor) must be kept low. Typically, the desirable limiting tensile stress for glass in a seal which must remain hermetic for its entire service life is about 10 MPa (~1500 Psi). Stresses in excess of 30 MPa (~4500 Psi) will surely cause some type of failure. Failure at stress levels between 10 and 30 MPa will depend upon other factors such as seal size, surface flaws in the metal or glass, internal flaws in the glass, or slow crack growth. Glass stressed above 10 MPa is also susceptible to fracture by subsequent processing and handling, such as when leads are attached to pins[18].

In addition to the compressive forces, there is generally a consideration of the chemical bonding of these seals. When certain pin, body, and glass materials are fused, there can be a chemical bonding which occurs. This provides additional integrity of a glass-to-metal seal.

1.3   Sealing Material

The combinations of eyelets, glasses and pins determine the integrity of a hermetic seal. Some common glass-to-metal seal combinations including corrosion - resistant glasses used in Lithium and Zinc-Silver Oxide battery applications are tabulated below. The selection of sealing glass for specific battery is very important. Corrosion - resistant glasses are widely used in $LiSO_2$ and $LiSOCl_2$, systems today[19]. Glasses like borosilicate grades are mostly used in $ZnAg_2O$. These specially formulated glasses are continuously growing to be used in other battery chemistries as manufacturers are designing systems for the highest reliability possible.

Table1.1: Some typical materials, including corrosion - resistant glasses, commonly used in glass-to-metal seals for lithium sulfur- dioxide and thionyl chloride batteries.

Body or eyelet	Glass	Pin material
Mild Steel	Ta-23, Fusite MSG-12, CABAL-12	Molybdenum, Tantalum, Tungsten
SS 304L	Fusite 435	SS 446, Alloy52, Titanium
Kovar	7056, 7052, DM305, etc	Kovar

1.4   Applications of Glass to Metal Seals

The market segments typically mentioned in relation to different battery application are: avionics, military, medical, industrial - commercial, and consumer. Each of these segments has specific needs and goals in relation to the performance of batteries

used in their application. These needs and goals are met by matching the various benefits that specific chemistries offer with the design and use considerations of the market. Following is a brief synopsis of each of these markets and some of the chemistries commonly used in their respective applications.

1.4.1 Avionics (Aerospace)

Avionics and aerospace, today is the rapidly developing field, which need high energy, high temperature, pulse activated in fraction of seconds, power source systems. Typical applications are in missiles, un-manned vehicles, space shuttles, in which the most common systems to be used are thermal and zinc silver oxide battery systems. Special glass metal seals are used in these systems and are high temperature and pulsed activated.

Thermal batteries (first developed by German scientists during WW II and were used in V2 rockets) are one-shot electrochemical power sources which remain inert until an internal charge of pyrotechnic is ignited, to melt and render conductive the normally solid electrolyte. These batteries used exhaust heat from the rocket to keep the electrolyte molten in the battery during their missions. They are mainly used in guided missiles in the fuses of various types of munitions and for certain emergency power needs in military aircraft. They serve to provide power to radar and electronic guidance as well as the guidance-fin motors. Some torpedoes and guided bombs depend on thermal and zinc silver oxide batteries for a power source.

1.4.2 Military

The military market has helped push the development of higher- energy power source systems in order to meet their wide range of needs; including applications such as:

communications systems, smart missiles, sonobuoys, mines, torpedoes, etc. The most common systems to be found in the military environment include lithium sulfur- dioxide ($LiSO_2$), lithium thionyl-chloride ($LiSOCl_2$), zinc-silver oxide battery systems (primary and rechargeable secondary both), nickel-cadmium systems and thermal battery systems etc. As in many technologies, the military has provided an avenue for manufacturers to develop new technologies and applications and prove these technologies through extensive field use.

The largest thermal batteries are used to provide emergency backup power for the hydraulic systems in military aircraft.

In all these applications, an efficient and good glass-metal seal is necessary to ensure the best performance of the devices.

1.4.3 Medical

The medical marketplace has experienced great success through adoption of lithium battery technology. Because of the long service life of lithium systems, products such as pacemakers and heart defibrillators now offer their users significant benefits over previous battery systems used in these applications. The most popular lithium chemistry used in the medical battery market has been lithium-iodine. Additional medical products that utilize lithium batteries are under development and are expected to experience significant growth in the future. These products include: drug-delivery systems (insulin, others), neuro stimulators, pumps, and portable diagnostic equipment[20].

1.4.4 Industrial – Commercial

The growth of different battery systems is having tremendous impact on the industrial-commercial, or OEM (Original Equipment Manufacturer) market. Because of

the variety of chemistries available, and the often non-interchangeable nature of these batteries with alkaline battery systems, OEMs are looking at lithium systems with great interest and care. Products can be designed smaller, have less weight, and operate considerably longer than with previous battery chemistries.

Applications within this segment include: memory backup for personal computers, utility consumption meters, cellular telephones, and a rapidly increasing raft of new products.

1.4.5 Consumer

The consumer marketplace for batteries is generally regarded as the over-the-counter retail trade. This is in contrast to the manufacturer of a consumer product supplying their goods with a battery as part of the package. These batteries are mostly button cells of different types e.g. CR1220, CR2016, CR2032, LR44 etc. used in calculators, computers, laptops, wrist watches etc.

1.5   Welding of Glass Metal Seal

In case of lithium batteries applications specifically, there are two distinct welding operations related to glass-to-metal seals. One is welding of the glass-to-metal seal into a battery lid, and the second is welding of the battery lid into the cane. Because of the economies of operations of glass-to-metal sealing, increasing the density or number of parts to be run through the oven decreases the cost per piece. For this reason, eyelets are often run through the oven to produce a glass-to-metal seal and are subsequently welded into a lid or battery cover assembly. This part is then ready to be welded into a battery cane to produce a hermetic battery cell.

General concerns when welding glass-to-metal seals include the selection of materials to be welded, and the heat shock to the seal during the welding process. Similar

metals should be chosen to be welded together whenever possible, as welding of dissimilar metals can contribute to corrosion at the weld interface.

The second aspect, of critical importance, is the heat shock to the glass seal. If too much temperature is produced, or too much force applied during welding, the glass may crack or have residual stresses and cause the battery to lose hermeticity. For this reason, a significant level of expertise in design and welding is needed.

In case of Zinc silver oxide battery applications, no such kind of welding is involved in the glass-metal sealing. As complete melting of glass bead after pre-sintering, to join with the metal part is sufficient for a good seal provided that sudden thermal shocks are avoided. These sudden thermal shocks cause subsequent cracks and other defects in the glass-metal seal thus affecting the efficiency and performance of the batteries.

1.6   Glass Classification

Glasses are classified as mineral inorganic, non-crystalline and polymeric or organic and crystalline glasses. Metallic glasses as in our case are the most important group of inorganic non-crystalline glasses. The structure of glasses may be considered on three scales:

1   The scale of 2 to 10 Å, or that local atomic arrangements;

2   The scale of 30 to few thousands Å, or that of sub microstructure;

3   The scale of microns to millimeters or more, or that of microstructure and macrostructure.

1.6.1   Glass Formation

Glasses are usually formed by solidification from the melt. The structure of glasses can be distinguished from that of liquids, since glass structure is independent of

temperature. The plot in fig (1.3) between specific volume vs. temperature shows this fact. On cooling the liquid, there is a discontinuous change in the volume at the melting point if the liquid crystallizes. If no crystallization occurs, the volume of the liquid decrease at about the same rate as above the melting point until there is a decrease in the expansion coefficient at a range of temperature i.e. the glass transformation temperature range. The glass structure does not relax at the cooling rate below this temperature range. The expansion coefficient for the glassy state is the same as that for the crystalline solid. By using slower cooling rates to increase the relaxation time for the structure, the super cooled liquid persists to a lower temperature, a higher-density glass results. Similarly, by heating the glassy material in the annealing range, in which slow relaxation occurs, the glass structure in time approaches an equilibrium density corresponding to the super cooled liquid at this temperature.
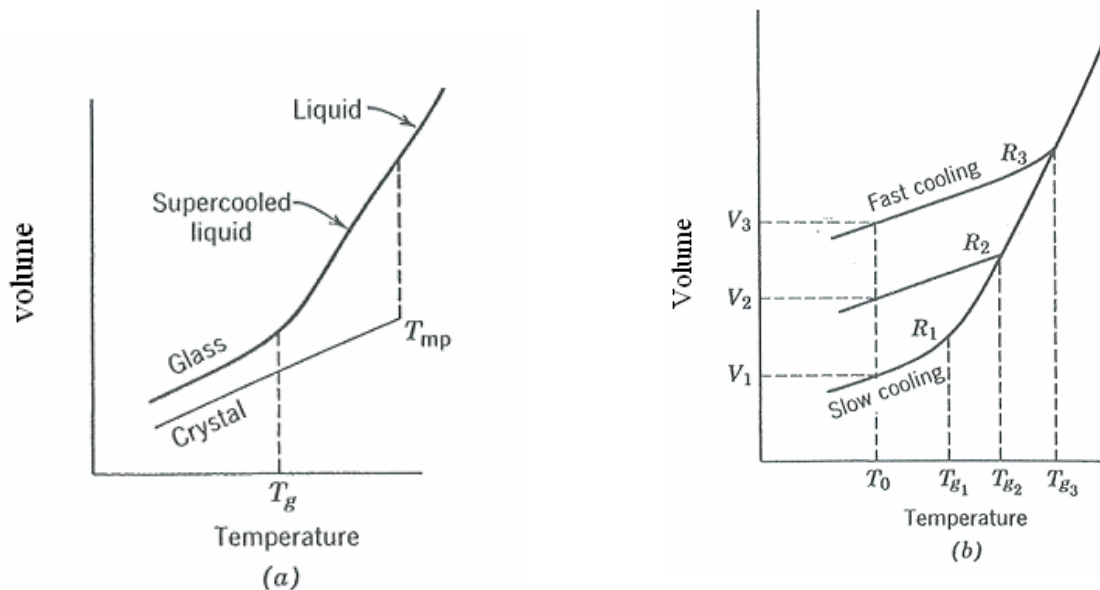
Figure 1.3: Schematic of specific volume-temperature relations. (a) Liquid, glass and crystal; (b) glasses formed at various cooling rates R1 < R2 < R3
(Courtesy: Introduction to Ceramics; second edition; Kingry, Browen, Uhlmnn)

The property of glass T_g, the glass transition temperature corresponds to the temperature of intersection between the curve for the glassy state and that for the super cooled liquid. Different cooling rates, corresponding to different relaxation times, gives rise to a different configuration in the glassy state equivalent to different points along the curve for the super cooled liquid. In the transition range, the time for structural re-arrangements is similar in magnitude to that of experimental observations. The configuration of the glass in this temperature range changes slowly with time towards the equilibrium structure. At higher temperatures the structure corresponding to equilibrium at any temperature is achieved very rapidly. At substantially lower temperatures, the configuration of the glass remains sensibly stable over long period of time.

As the liquid is cooled from a higher temperature without crystallizing, a region of temperature is reached in which a bend appears in the volume-temperature relation. In this region the viscosity of the material increases to a sufficiently high value, typically about 10^{12} to 10^{13} P, so that the sample exhibits solid-like behavior. As shown in figure, the glass transition temperature increases with increasing cooling rate, as do the specific volumes of glasses which are formed. The specific volume of the glass at temperature T_o can be V_1, V_2 or V_3 depending on the three cooling rates used in forming the glass.

Non-crystalline solids can be formed in other ways besides cooling from liquid state, and their structure may differ significantly from glasses formed by the cooling of liquids. One of these methods is condensation from a vapor onto a cold substrate. When a vapor stream formed by electron beam evaporation, sputtering, or thermal evaporation impinges on the cold substrate, thermal energy is extracted from the atoms before they can migrate from to their lowest free-energy states (crystalline state).

Another method of forming glass is by electro-deposition; e.g. Ta_2O_5, Ge and certain Ni-P alloys. Non-crystalline solids can also be formed by chemical reaction. Silica gel is prepared from the reaction of Ethyl silicates.

1.6.2   Structure of Oxide Glasses

Recent advances in experimental techniques and means of analyzing data have opened a new era of glass-structure studies.

1.6.2.1   Silica Glass

From the width of the main broad diffraction peak in the glass diffraction pattern, the crystallite size in the case of SiO_2 was estimated at about 7 to 8 Å. Since the unit cell of cristobalite is also about 8 Å, any crystallites would be only a single unit cell in extent; and such structures seem at variance with the notion of a crystalline array. This remains a powerful argument even if the estimate of crystallite size were only accurate to within a factor of 2. There is no marked small-angle scattering from a sample of fused silica in contrast to silica gel (fig 1.4). This indicates that the structure of the glass is continuous and is not composed of discrete particles like the gel. Hence if crystallites of reasonable size are present, there must be a continuous spatial network connecting them which has a density similar to that of the crystallites.

A more recent X-ray diffraction study of fused silica was carried out with advance experimental techniques and means of analyzing data. The distribution of Si-O-Si bond angles was determined (fig 1.4b). These angles are distributed over a broad range, from about 120 to 180°, centered about 145°. This range is much broader in the glass than in the corresponding distribution for crystalline cristoballite. In contrast, the Si-O and O-O distances are nearly as uniform in the glass as in the crystal.

The essential randomness of the SiO_2 glass structure results from a variation in the Si-Si

distances (the Si-O-Si bond angles). Beyond this direct joining of the tetrahedra over a

range of Si-O-Si angles, the structure of fused silica is completely random. That is there

appears no pronounced preference in fused silica for edge to face sharing of tetrahedral,

which is found in crystalline silicates.

The structure of fused silica is then described well by a random network of SiO_4

tetrahedra, with significant variability occurring in Si-O-Si bond angles.
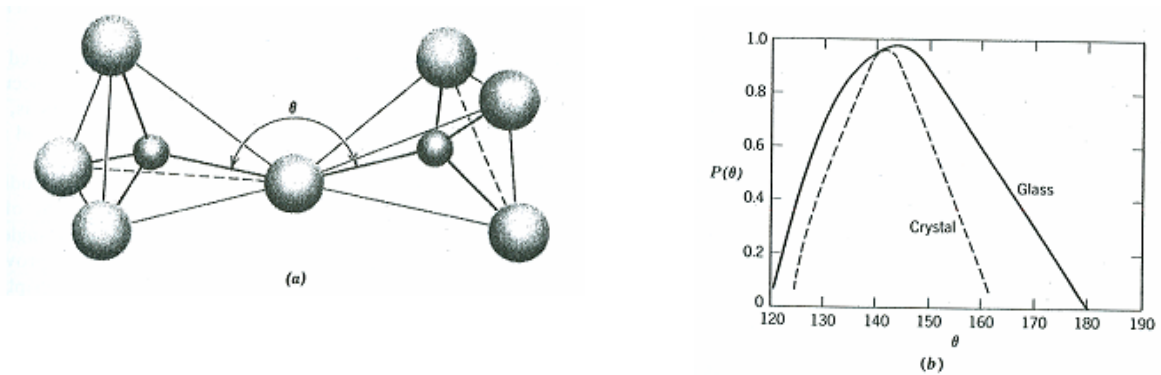
Figure 1.4: (a) Schematic representation of adjacent SiO_4 tetrahedra showing Si-O-Si bond angle. Close circles – Si; Open circles- O; (b) distribution of Si-O-Si bond angle in fused silica and crystalline cristobalite. From R.L. Mozzi, Sc. D. thesis, MIT, 1967

1.6.2.2 B_2O_3 Glass

X-ray diffraction and NMR of glassy B_2O_3 clearly indicates that the structure is

composed of BO_3 triangles. A random network of triangles linked together in the

structure, provides a poor representation of the diffraction data. A better description is

provided by a model in which the triangles are linked in a boroxyl configuration fig

(1.5). A better model is based on a distorted version of the crystal structure in which the

triangles are linked in ribbons. The distortions are such as to destroy the essential

symmetry of the crystal, and the notion of discrete crystallites embedded in a matrix is not appropriate.
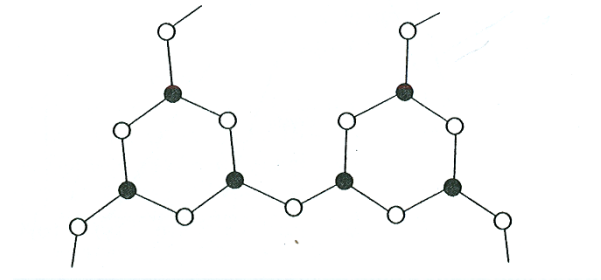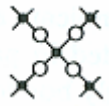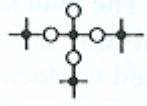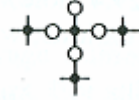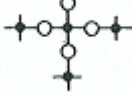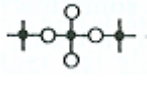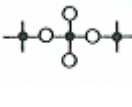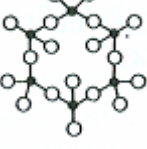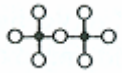
Figure 1.5: Schematic representation of boroxyl configuration. Filled circles- B, Open circles- O: (From R.L. Mozzi, and B.E. Warren, *J. Appl. Cryst.*, 3, 251 (1970))

1.6.2.3   Silicate Glasses

The addition of alkali or alkaline earth oxides to SiO_2 increases the ratio of oxygen to silicon to a value greater than 2 and breaks up the three-dimensional network with the formation of singly bonded oxygen which does not participate in the network. Table 2 shows this network, its structure and models. For the reasons of local charge neutrality, the modifying cations are located in the vicinity of the singly bonded oxygens. With divalent cations, two singly bonded oxygens are required for each cation; for univalent alkali ions, only one such oxygen is required.

An X-ray diffraction study of a number of K_2O-SiO_2 glasses indicates systematic changes in the structure as the alkali oxides are added to SiO_2.

Table 1.2: Effects of O-Si ratio on silicate network structure. Models are also shown for reference. (Courtesy: Introduction to Ceramics; second edition; Kingry, Browen, Uhlmann)

Ratio O/Si	Structure	Model		
2.0	Network (SiO_2)			
2-2.5	Network			
2.5	Network			
2.5-3	Network, Chain or Rings			
3.0	Chain and Rings			
3-3.5	Chain, Rings and Pyrosilicate ions			
3.5	Pyrosilicate ions			
3.5-4	Pyrosilicate ions and Orthosilicate ions			
4.0	Orthosilicate ions			

1.6.2.4　　　　Borate Glasses

The addition of alkali or alkaline earth oxides to B_2O_3 results in the formation of BO_4 tetrahedra. The variation of the fraction of four-coordinated boron's with the concentration of alkali oxides is shown in fig (1.6). The smooth curve shown in the figure represents that each of the oxygen added with the alkali ions converts two triangles to tetrahedra. Up to alkali oxide concentration of about 30 mole %, nearly all the modifier oxides have the effect of converting BO_3 triangles to BO_4 tetrahedra. Beyond this composition range, the experimentally determined fractions of four coordinated boron depart significantly from the curve, so singly-bonded oxygen are produced in appreciable numbers.
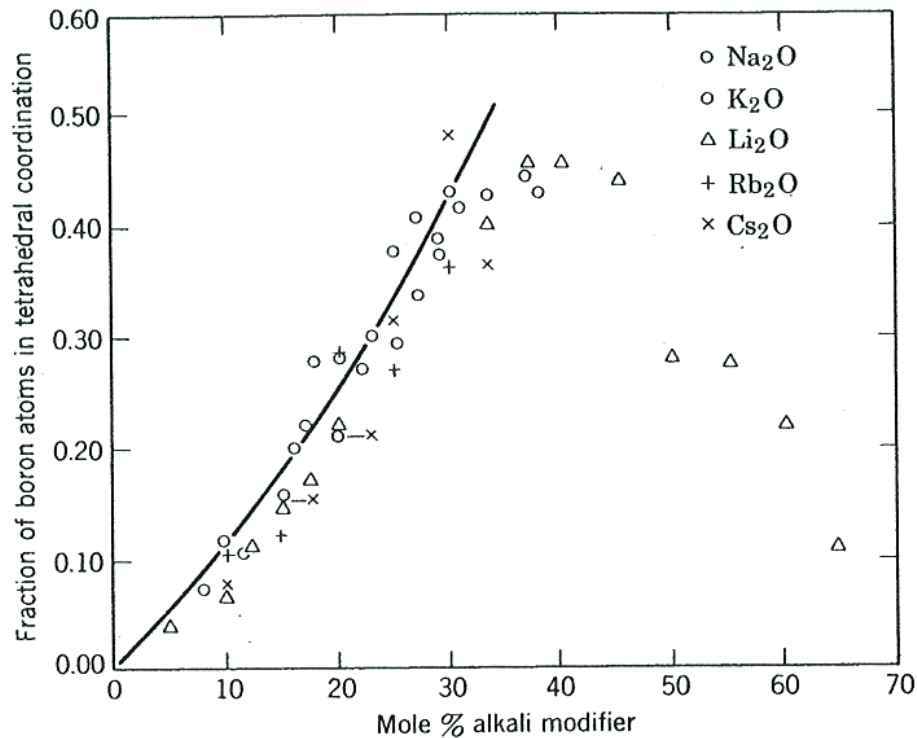
Figure 1.6: The fraction of Boron atoms in BO_4 configuration in alkali borate glasses plotted against molar percent of alkali oxide. (Form P.J.Bray, Interaction of Radiation with Solids, Plenum Press, New York, 1967)

1.6.3 Selection of Glasses for Glass to Metal Seal

The selection of a glass used in sealing applications is typically dependent on the body and pin materials that will be fused with the glass to form a seal. Batteries require a specially formulated corrosion - resistant glass is used to form a seal with long-life reliability. Glass corrosion in a battery system can lead to failure of the battery from short-circuiting across the seals and/ or from cracking of the glass, there by permitting leakage of the battery electrolyte material. Short-circuiting occurs as corrosion forms on the glass and creates a conductive bridge across the glass, or insulator.

1.7   The Kovar Alloy

Kovar is an iron-nickel-cobalt alloy with a coefficient of thermal expansion similar to that of hard (borosilicate) glass. This makes it especially suitable for uses which require a matched-expansion seal between metal and glass parts. Thus kovar finds wide usage in the electronics industry for metal parts bonded to hard glass envelopes for such devices as power tubes, x-ray tubes, etc., and other applications requiring glass-to-metal seals.

1.7.1   Heat Treatment of Kovar Alloy

The heat treatment of the material results in ensuring optimum conditions for glass sealing, plating or brazing. The oxidation upto a specified limit to gain some oxide layer on the surface of the metal as a result of heat treatment of the Kovar is the most beneficial state in achieving excellent seal between the glass and the Kovar.

1.7.2 Typical Properties of Kovar Alloy:

Table 1.3: Some typical properties of Kovar alloy are tabulate as follows:

Physical Properties		
1	Density (lb/in^3)	0.302
2	Specific Gravity:	8.36
3	Curie Temperature ^{o}C	435
4	Melting Point ^{o}C	1450
5	Specific Heat (Cal/gm/ ^{o}C) At 0 ^{o}C, 430 ^{o}C	0.105, 0.155
6	Heat of Fusion (Cal/gm)	64
7	Thermal Conductivity (W/m · K)	17.3
8	Electrical Resistivity (μ ohm/mm)	490
Typical Mechanical Properties		
1	Shear Modulus	7.5 x 10^6
2	Modulus of Elasticity	20 x 10^6
3	Ultimate Strength: (psi)	75000
4	Yield Strength (psi)	50000
5	Kink Point ^{o}C	430
6	Poisson's Ratio:	0.317
7	Elongation	30%
8	Velocity of Sound (ft/sec)	16300
9	Hardness (Rockwell B)	78
Coefficient of Thermal Expansion (CTE) x 10^6 m/m-K		
1	30-900 ^{o}C	4.9-11.5

1.8   Sintering of Glass Powders

Pre-sintering and post sintering of the glass powders are important processes in making the glass beads and the final glass-metal seals in the sintering furnace at various temperatures. Sintering is described as the process by which small solid particles are bonded together i.e. agglomerated by diffusion. This thermal treatment results in transformation of a porous compact in a dense coherent product. Simply we say that sintering is the bonding together of particles at high temperatures. It can occur at temperatures below the melting point by solid-state atomic transport events, but usually involve the formation of a liquid phase. On a micro structural scale the bonding occurs as cohesive necks grow at the particle contacts. Or it is a thermal process which creates inter-particle welds, improving upon properties observed in the green state. Sintering in our case is important because our joining media are in two different modes i.e. we are required to make an efficient seal between a glass powder in the form of bead and a metal, Kovar pin. There must be some mechanism (s) for material transport and a source of energy to sustain this material transport.

During the usual processing of compaction of the glass (non crystalline) powders, crystalline powders and ceramics, they are fired at a temperature sufficient to develop useful properties. During the firing process, changing may occur initially because of decomposition or phase transformation in some of the phases present. On further heating the fine-grained, porous compact, three major changes occur.

1   An increase in grain size and shape

2   Change in pore shape

3   Change in pore size and number to give a decreased porosity

1.8.1   Pore Structures during Sintering

A powder compact may compose of individual grains separated by 25 to 60 vol % porosity, depending on the particular material used. In order to maximize properties, it is necessary to eliminate as much of this porosity as possible. These results are obtained during firing by the transfer of material from one part of the structure to the other. Figure (1.7) illustrates the changes that occur during a firing process. The pores initially present can change shape but more commonly, both the shape and size of the pores change during the firing process. Starting with particles in point contact at the initial stage that grows into necks, the grain boundary and the pore configuration controls the sintering rate. At the beginning of the intermediate stage, the pore geometry is highly convoluted and the pores are located at grain boundary intersections. With continued sintering, this geometry approaches a cylindrical shape where densification occurs by decreasing the pore radius.

In the latter stage of sintering, intersection between pores and grain boundaries can take three forms, the pores can retard grain growth, they can be dragged by the moving grain boundaries during grain growth or the grain boundaries can break away from the pores, leaving them isolated in the grain interiors. At the typical sintering temperatures, most materials exhibit moderate to high grain growth rates. As the temperature is increased, the rate of grain growth and grain boundary motion increases to a point where the boundaries break away from the pores. At low temperatures, the rate of grain growth is small so the pores remain attached and cause to obstruct the grain growth.
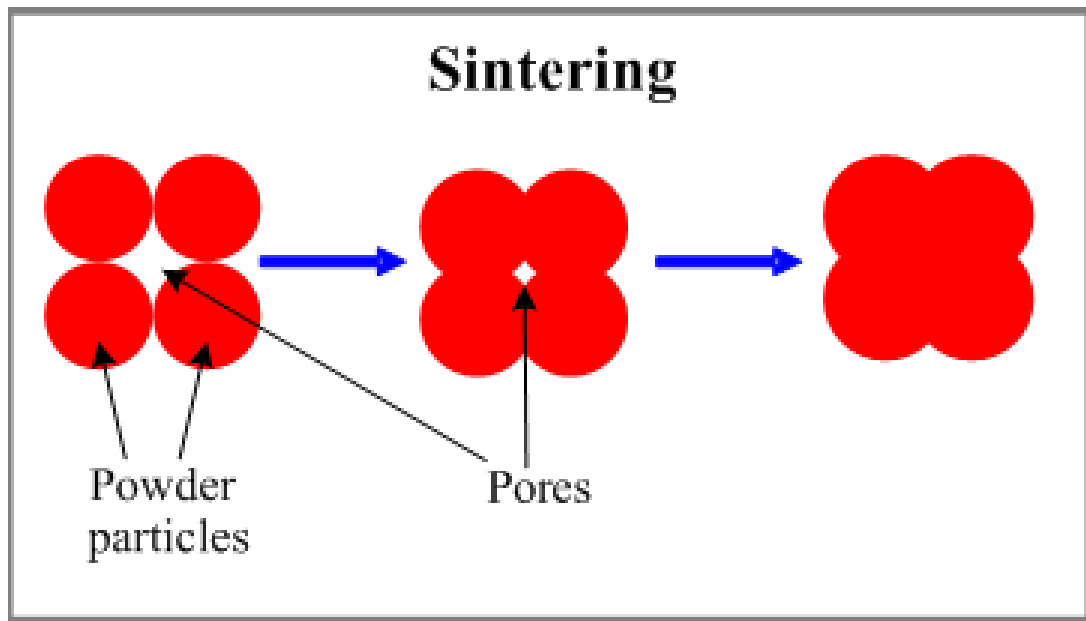
Figure 1.7: Schematic diagram of changes in pore shape. The diagram shows that changes in pore shape do not require shrinkage.
(Source: www.substech.com)

1.8.2 Deriving Force for Densification in Sintering

The changes in free energy that give rise to densification are due to the decrease in surface area and lowering of the surface free energy due to the elimination of solid-vapour interfaces. This is however, accompanied by the generation of a new but lower energy solid-solid interface.

Material transfer is affected by the pressure difference and change in free energy across a curved surface on microscopic scale. These changes are due to surface energy. If the particle size and consequently the radius of curvature are small, these effects may be of substantial magnitude. They become very large, when the radius of curvature is less than a few microns. This is the reason for using fine particle of glasses and ceramics.

1.8.3 Material Transport during Sintering

Since the deriving force is the same in all systems, the various mechanisms of material transport are:

1.8.3.1 Vapor-Phase Material Transport (Evaporation-Condensation)

During the material transport process, there is tendency for the material to transport between various parts of the system because of the difference in surface curvature. This results in difference in vapour pressure at various parts. This is important in few systems. By considering the initial stages of the process when the powder compact is just beginning to sinter and concentrate on the interaction between two adjacent particles (fig 1.8). At the surface of the particle, there is a positive radius of curvature, so that the vapour pressure is somewhat higher than would be observed for a flat surface. However, just at the junction between particles, there is a neck with a small negative radius of curvature and a vapor pressure an order of magnitude lower than that for the particle itself. The vapor pressure difference between the neck area and the particle surface tends to transport the material into the neck area.

Distance between centers of spherical particles is not affected by vapour material transfer and that only the shape of the pores is changed. This process therefore does not affect density and shrinkage of a row or compact of particles.

The rate of pore shape change is affected by time, initial radius of the particle and the vapour pressure. The vapour pressure increases exponentially with temperature and therefore the vapour-phase sintering process is strongly temperature dependent. The control variables are usually the initial particle size and the temperature.
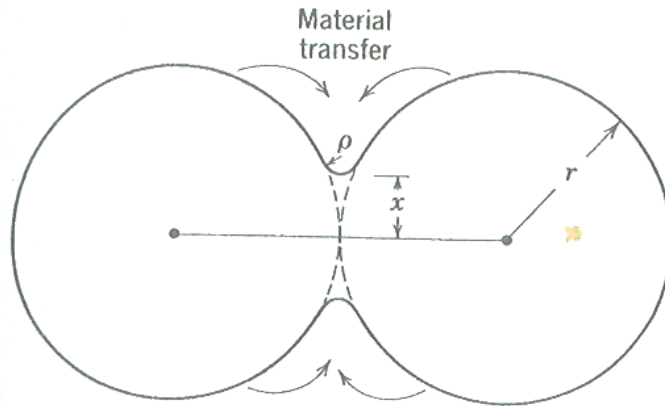
Figure 1.8: Schematic diagram of the initial stages of sintering by evaporation-condensation. It is clear that the material transfers towards the neck from the surface. (Courtesy: Introduction to Ceramics; second edition; Kingry, Browen, Uhlmann)

1.8.3.2   Solid-State Material Transport Processes

The difference in free energy or chemical potential between the neck area and the surface of the particle provides a deriving force for the transport of material by the fastest means available. If the vapour pressure is low, material transfer may occur by solid-state processes. In addition to vapour transport, matter can move from the particle surface, from the particle bulk, or from the grain boundary between particles by surface, lattice, or grain boundary diffusion. All these processes are parallel methods of lowering the free energy of the system. Figure (1.9) and Table 1.4 best describes all these processes. These processes contribute significantly towards sintering.

The transfer of material from the surface to the neck by surface or lattice diffusion, like vapour transport, does not lead to any decrease in the distance between particle centers. These processes do not result in shrinkage of the compact and a decrease in porosity. Only transfer of matter from the particle volume or from the grain boundary between particles causes shrinkage and pore elimination.

Table 1.4: Alternate paths for matter transport during the initial stages of Sintering

Mechanism Number	Transport Path	Source of Matter	Sink of Matter
1	Surface diffusion	Surface	Neck
2	Lattice diffusion	Surface	Neck
3	Vapour transport	Surface	Neck
4	Boundary diffusion	Grain boundary	Neck
5	Lattice diffusion	Grain boundary	Neck
6	Lattice diffusion	Dislocations	Neck
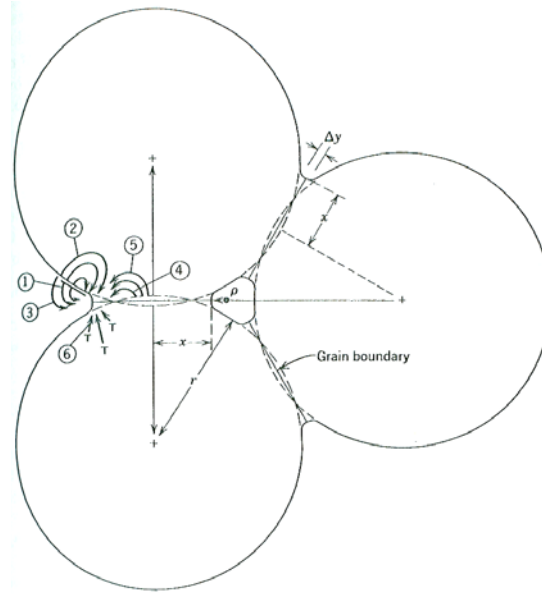
Figure 1.9 Schematic diagram of the sintering showing the alternate paths for matter transport during the initial stages of sintering
(Courtesy: Introduction to Ceramics; second edition; Kingry, Browen, Uhlmann)

Sintering rate decreases with time, so sintering for longer time periods to obtain improved properties is impracticable. Therefore time is not a critical variable for process control. Control of particle size is very important, since the sintering rate is roughly proportional to the inverse of the particle size. For large particles even long periods do not cause extensive sintering, as the particle size is decreased, the rate of sintering is raised.

Diffusion co-efficient is another control which is affected by composition and temperature. Diffusion path is affected by microstructure. Surface diffusion is most

important in the early stages of sintering (these affect the neck diameter between particles but not the shrinkage and porosity). Grain boundary diffusion and volume diffusion subsequently become important. In general, the presence of solutes which enhance either boundary or volume diffusion coefficients enhance the rate of solid-state diffusion. Both volume and boundary diffusion coefficients are strongly temperature-dependent which means that the sintering rate is dependent on the temperature level.

In order to effectively control sintering process which takes place by solid-state process, it is essential to maintain close control of the initial particle size and particle size distribution of the material, the sintering temperature, the composition and the sintering atmosphere.

1.8.3.3 Liquid Phase Sintering

In two phase systems involving mixed powders, it is possible to form a low melting phase. In such a system, a liquid provides a rapid transport for a rapid sintering. Wetting is the first requirement, as the liquid must form a film around the solid phase. A wetting liquid has a small contact angle, θ defined as

$$\gamma_{sv} = \gamma_{sl} + \gamma_{lv} \cos (\theta)$$

Where γ_{sv} is the solid-vapour surface energy, γ_{sl} is solid-liquid surface energy, and γ_{lv} is the liquid-vapour surface energy. A small contact angle indicates that the liquid will spread over the solid surface. The solid must be soluble in liquid. Finally, the diffusive transport for the dissolved solid atoms should be high enough to ensure rapid sintering. The liquid film provides a surface tension force to aid densification. In liquid phase sintering, the densification rate is much higher than in solid-state sintering, and times as short as 15 minutes at the maximum temperature can successfully produce full density.

1.9   Diffusion at Glass-Metal Interface

The glass particles come closer to each other to form a compact by the process of sintering or more specifically by diffusion. Diffusion is the key mechanism involved at the glass to metal interface. For a crystalline solid, nearly every particle contact evolves a grain boundary with associated grain boundary energy. The grain boundaries are defective regions with high atomic mobility. The sintering mechanism describes the path of atomic motion which produces the mass flow. For metal powders these mechanisms are called diffusion processes over the surfaces, along the grain boundaries, or through the crystalline lattice. Diffusion is thermally activated, meaning that specific energy is necessary for atomic movement. Motion depends on its current site and move into a vacant site. There is an intermediate position of high energy when the atom moves from one lattice site to another by the diffusion jump. The population of vacant atomic sites and the number of atoms with sufficient energy to move into these sites varies with the Arhenius temperature relation,

$N/N_o = \exp(-Q / RT)$,

Where N/N_o is the ratio of available sites or activated atoms to total atoms, Q is the activation energy, R is gas constant and T is absolute temperature.

1.9.1   Atomic Measurements of Diffusion

The diffusion of atoms through a solid can occur in two mechanisms which depend on the type of site occupied in the lattice. These are substitutional atoms and the smaller interstitial atoms. The former diffuse by a mechanism of vacancy while the latter migrate by forcing their way interstitially between the larger atoms

Normally a substitutional atom in a crystal oscillates about a given site and is surrounded by neighboring atoms on similar sites. The movement of a substitutional atom

is limited by its neighbors and the atom cannot move to another site. If an adjacent site is vacant, it may happen that a particular violent oscillation results in the atom jumping over on to the vacancy.

So the probability that any atom will be able to jump into a vacant site depends on the probability that it can acquire sufficient vibrational energy. The rate at which any atom is able to migrate through the solid will clearly be determined by the frequency with which it encounters a vacancy and this in turn depends on the concentration of the vacancies in the solid. Both the jumping and concentration of the vacancies are extremely sensitive to the temperature.

When the solute atom is appreciably smaller in diameter than the solvent, it occupies one of the interstitial sites between the solvent atoms. As in FCC materials, the interstitial sites are in the middle of the unit cell, these are octahedral sites. In the BCC lattice, the interstitial atoms also occupy the octahedral sites, which are located at edge-centering or face-centering positions.

CHAPTER 2

THE CHARACTERIZATION TECHNIQUES

During the course of this research work, various instrumental analyses were made using XRF, SEM-EDS, XRD, DSC, GAS PYCNO METER, TGA etc. The differential scanning calorimetry is utilized to study the thermal transitions. To reveal the crystallographic nature, X-ray diffraction has been carried out though the information extracted is limited. Sophisticated micrographs were revealed using the characterization techniques of SEM. The useful tool of XRF was beneficial in finding the compositional analysis of the samples during the entire experimental work. These techniques proved to be very helpful in analyzing the glass powders, to get the insight of various samples of glass beads, and the final product etc. Some of these techniques are SEM-EDS, TGA, XRD, and DSC etc are described briefly for reader reference.

2.1   Scanning Electron Microscopy

This is a surface imaging technique based upon the utilization of secondary electron beam. SEM provides higher magnification with greater depth resolution than optical microscopes. SEM images may become distorted by the surface potential that builds up on insulators or edge effects at sharp contours. Insulators may be coated with a thin (~100Å) conductive layer to dissipate the surface charge. SEM images at less than 20Å resolution have been obtained with several hundred thousand times magnification.

2.1.1   Working Principle

Electrons with energies 40keV in the form of fine 'probe' are focused at the surface of specimen. Among the different phenomenon at the surface under electron

impact, backscattering of high energy electrons and emission of secondary electrons with few electron volts energy are more important for scanning electron microscopy. The angle of reflection of both backscattered and secondary electrons depend upon the topographical features of the specimen surface and the intensity of emission is very sensitive to the angle at which the electron beam strikes the surface. The emitted electron current is collected and amplified; variations in the resulting signal strength are used to vary the brightness of the trace of a cathode ray tube being scanned in synchronism with the probe. There is thus a direct positional correspondence between the electron beam scanning across the specimen and the fluorescent image on the cathode ray tube.
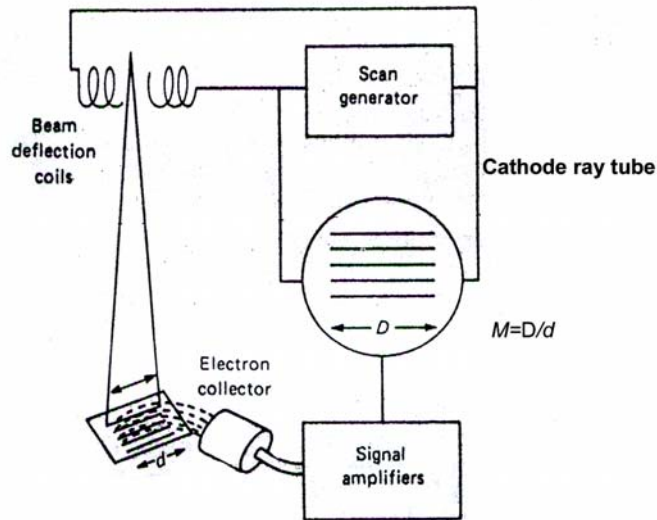
Figure 2.1: Schematic diagram showing the principle of scanning electron microscope. (Mazher et al.)

2.1.2 Magnification

The magnification produced by a scanning microscope is the ratio between the dimensions of the final image display and the field scanned on the specimen. Changes in magnifications are brought about by altering the extent of scan on the specimen whilst

keeping the size of display constant. In practice magnification switch on the microscope actually varies the angle through which the beam is reflected; the linear extent on the scan depends on the working distance of the specimen from the final lens.

Figure 2.2: Scanning Electron Microscope with opened sample chamber (Courtesy: Wikipedia, the encyclopedia).

2.1.3   Resolving Power of SEM

In the SEM object detailed is sampled point by point and the resolving power of the instrument is directly influenced by the smallest area which in can sample, i.e. by the diameter of the probe. Minimizing the probe diameter calls for a lens system with small aberrations and high electrical stability. Better resolving power is only obtainable by working with a stronger lens or brighter electron source. In SEM the practical resolution in secondary and backscattered electron images will generally be poorer than the probe diameter would suggest, because the electron beam penetrates and diffuses sideways in the specimen, releasing electrons from wider area than that actually illuminated by the focused probe. Practical resolution of detail in bulk specimens is dependent on the nature of specimen, its orientation in microscope, the working distance and the recording of the final image. It is not a quantity which is not amenable to the conventional Airy disc/

Rayleigh criterion for microscope systems and there is as yet no accepted standard for measuring or comparing the resolving powers of scanning microscopes.

2.1.4 Image Recording on the SEM

The SEM image is recorded sequentially, generally by photographically the face of cathode ray tube in a time exposure as the image is drawn on it line by line for one complete frame. It is usual to record from a tube with a screen coated with a blue phosphor (P11) with a short resistance, having a higher resolution than the yellow-green phosphor (P7) of the 'visual' tube. The 'record' tube has its own brightness and contrast controls which can be set to suit the characteristics of photographic material being used for recording. The image is scanned with more lines per picture than the screen can resolve, so that no scanning lines are seen in the photographic record. The 'record' scan is made more slowly than the visual scan used for selection and focusing, in order to give a smoother, grain-free micrograph. The frame time in recording may be between 30 and 200 seconds, depending on how 'noisy' the image is. High magnification images made with small focused probes will require the longer times since signal-to-noise ratio will be low. Under these conditions, too, the image may be grainy for TV rate scanning to produce a recognizable image, and slow scanning will be the order of the day all round.

The photographic record may be made on negative film of 35mm or larger format; alternatively instant prints may be made on Polaroid-type material. It is increasingly common for essential data such as exposure number and magnification recorded on the film at the same time. Although the earlier stereo-scans and certain other microscopes used a square picture format on a picture tube 100mm square, this is a less practical shape than a rectangular 'landscape format. Most current SEM's produce a

picture which is rectangular and compatible with the 1:1.25 aspect ratio of 4"× 5" photographic material.

The manner of recording leads to one important difference micrographs made in the TEM and SEM. It is generally to enlarge a portion of a well focused transmission micrograph to examine a particular feature in greater detail, since the electron image contains all the resolution of which the microscope is capable, and the photographic emulsion on which it falls is very fine-grained. A scanning micrograph, however, will only contain image detail which is comparable with the grain size of Phosphor of the recording tube; finer structure than this must be magnified in the microscope at the time of taking, and can not be obtained by photographic enlargement afterwards. In other words it is normally pointless to use a magnifying glass on a scanning micrograph already enlarged to, say, twice the size of the record screen. The visual impact of a larger print, as distinct from its information content, is a different matter.

It is also possible to obtain images of magnetic domains in an SEM. Small sub-grain sized regions called domains are found in ferromagnetic materials. The magnetic moment of these domains may be along a certain crystallographic axis. In some crystals, a magnetic moment component is often normal to the surface. This surface magnetic moment is able to exert a force on the secondary electrons ejected from the surface of a uni-axial crystal. As the sign of local magnetic flux changes over each domain, that affects the secondary electron signal. Therefore images of domains can be obtained using a secondary electron detector.

Similarly, in case of ferromagnetic crystals, there is more than one preferred axis and a primary electron will experience a force in different directions from domain to domain.[21]

One of the most common analytical attachments to the SEM is the energy dispersive x-ray spectrometer (EDS). The useful energy range for EDS systems is from 1.0 to 220 keV, which limits the analysis to elements with $Z > 9$. EDS detectors with thin protective layers or without protective layer, when used in ultra-high vacuum systems, permit analysis of the lighter elements down to B. The analysis depth is dependent on the path length of the x-rays, not the primary electron beam. As a result, EDS signals may originate from depths of 0.5 μm or more.

Due to pulse counting mode of EDS system, it has ability to detect the characteristic x-rays for all elements above F in the periodic table. Therefore, EDS system takes much shorter time to scan the complete spectrum as compared with wavelength dispersive x-ray (WDX) analyzer. Moreover, EDS analyzer has a resolution of approximately 150eV, whereas a WDX analyzer has a resolution of 5eV. The detector used with EDS is of Li-doped Si that requires liquid nitrogen cooling to keep the Li from diffusing and rapidly degrading the detector's performance.[22]

2.1.5   The SEM Advantages

The SEM has compensating advantages including,

- The ability to image a comparatively large area of the specimen;

- The ability to image bulk materials (not just thin films or foils);

- The variety of analytical modes available for measuring the composition and nature of the specimen.

- Depending on the instrument, the resolution can fall somewhere between less than 1 nm and 20 nm.

2.2 Differential Scanning Calorimetry (DSC)

One of the fundamental concepts of modern sciences and the basis of thermodynamics is the connection between heat and energy. An entire class of materials analysis techniques is based on the ability to transfer heat to a material and monitor the effects. This class of techniques is known as thermal analysis. Differential Scanning Calorimetry (DSC) is a convenient and highly accurate method for performing thermal analysis on a wide variety of materials. Phase transformation temperatures, enthalpies of transformation and thermal transitions hysteretic data of a sample can be determined by measuring the heat flow of the sample compared to a reference material. DSC is a technique for measuring the energy necessary to establish a nearly zero temperature difference between a substance and inert reference material, as the two specimens are subjected to identical temperature regimes in an environment heated or cooled at a controlled rate.

The PerkinElmer DSC instrument is used for the thermal characterization of metallic glasses in the present study. A schematic representation of this instrument is shown in Fig. 2.3. The temperature difference is kept equals to zero by placing the temperature sensors, Pt resistor thermometers into a bridge circuit. Any imbalance is used to drive a heater in the appropriate sample or reference portion of the cell. The power required to keep the bridge circuit in balance is proportional to the change in heat capacity or enthalpy occurring. The reaction is endothermic if the power is supplied to the sample and exothermic when it is supplied to the reference.
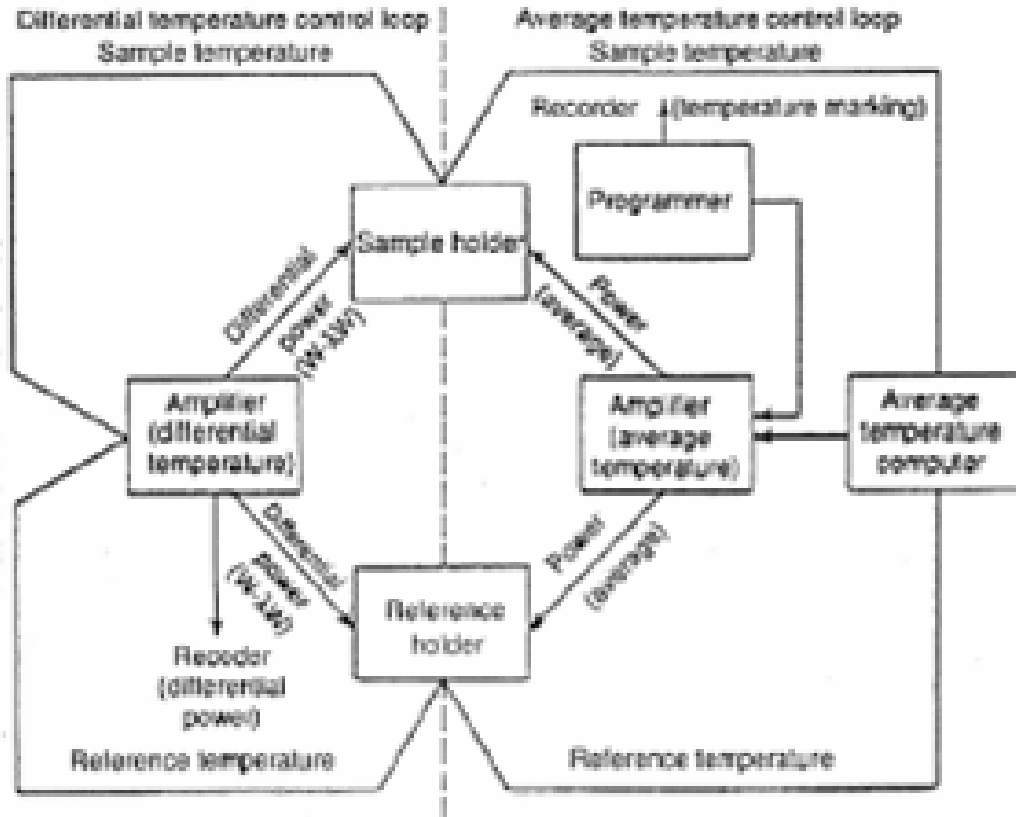
ure 2.3: Schematic representation of the operation of power compensating DSC instrument [Watson64].

2.3   Types of DSC System

There are two types of DSC systems in common use

2.3.1   Power Compensation DSC

In power-compensation DSC the temperatures of the sample and reference are controlled independently using separate, identical furnaces. The temperatures of the sample and reference are made identical by varying the power input to the two furnaces; the energy required to do this is a measure of the enthalpy or heat capacity changes in the sample relative to the reference. Schematic diagram of the power compensation DSC is shown in fig.2.4
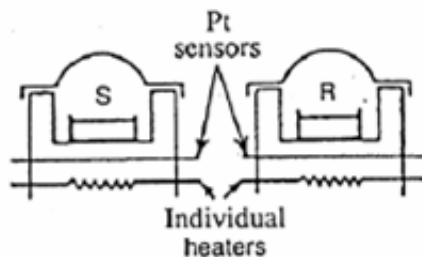
Figure 2.4: Schematic diagram of Power Compensation DSC showing the main component, e.g. individual heaters, Pt sensors etc. (Shariq et al.)

2.3.2 Heat Flux DSC

In heat-flux DSC, the sample and reference are connected by a low resistance heat flow path (a metal disc). The assembly is enclosed in a single furnace. Enthalpy or heat capacity changes in the sample cause a difference in its temperature relative to the reference. The temperature difference is recorded and related to enthalpy change in the sample using calibration experiments. Schematic diagram of heat flux DSC is shown in fig 2.5.
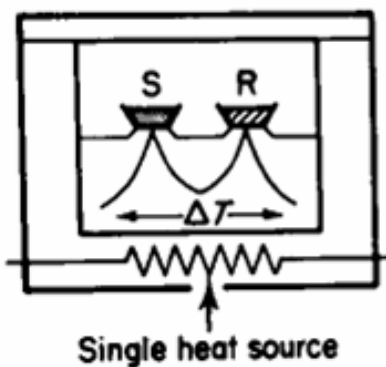
Figure 2.5: Schematic diagram of Heat flux DSC that shows a single heat source. (Shariq et al.)

In heat flux DSC system, the main assembly of the DSC cell is enclosed in a cylindrical, silver heating block, which dissipates heat to the specimens via a constantan disc which is attached to the silver block. The disc has two raised platforms on which the

sample and reference pans are placed. A chromel disc and connecting wire are attached to the underside of each platform, and the resulting chromel-constantan thermocouples are used to determine the differential temperatures of interest. Alumel wires attached to the chromel discs provide the chromel-alumel junctions for independently measuring the sample and reference temperature. A separate thermocouple embedded in the silver block serves a temperature controller for the programmed heating cycle.

An inert gas is passed through the cell at a constant flow rate of 40 ml min^{-1}. The thermal resistances of the system vary with temperature, but the instruments can be used in the `calibrated' mode, where the amplification is automatically varied with temperature to give a nearly constant calorimetric sensitivity.

2.5   X-Ray Diffraction

X-ray diffraction is one of the most important tools of solid-state science as a matter of the fact that it constitutes a powerful and readily available method for determining atomic arrangements in matter. These techniques cover various investigations, including qualitative and quantitative phase identification and analysis, differentiating between crystalline and amorphous materials, determination of the crystalline structure (crystal axes, size and shape of the unit cell, positions of the atoms in the unit cell), determination of the orientation of single crystals, determination of the texture of poly-grained materials, measurement of strain and small grain size, measurement of various kinds of randomness, disorder, and imperfections in crystals and determination of radial distribution functions for amorphous solids and liquids.

Since many electric and electronic properties are determined by the crystalline structure of thin films, X-ray diffraction method is preferred for the thin film analysis. A wide

range of different X-ray diffraction techniques and instruments are available for thin film characterization, each method having its own application and advantage. Powder x-ray diffraction technique is helpful in determining the crystalline nature of thin film, extent of crystallinity and identification of crystalline phase(s). The diffraction pattern generated allows determining the chemical compound or phase composition of the film, the texture of the film (preferred alignment of crystallites), the crystallite size and presence of film stress.

Crystal structure is difficult to resolve for the systems other than simple high symmetry crystals. Accordingly, it is mostly used as a finger print method for detecting the presence of a known compound or phase in a product. A huge library of powder patterns of known compounds is present as JCPDS (Joint Committee for Powder Diffraction Standards) files. When the powder pattern of the sample has been measured and both the d_{hkl} spacing and intensity of the lines recorded, these can be matched against the patterns of known compounds in the files.

The qualitative analysis and purity check of the sample is possible. However it does not work for amorphous samples or if the impurity increases more than 5%

Powder diffraction can be used for differentiating mixture of small crystals, determining phase diagrams and deciding whether different metal containing structures are isomorphous.

2.5.1 Working Principle

When high speed electrons accelerated in large potential difference of 20-25KeV are allowed to impact on a target metal, target or anode emit a continuous spectrum of white x-radiation. In addition sharp, intense K_{α}, K_{β} line are also superimposed whose

frequencies are characteristics of the anode metal. The energy of bombarding electrons are enough to knockout the K-shell electrons producing vacancies for higher shell electrons. The decrease in energy appears as radiation; electrons from L-shell are responsible for K_α line and from M-shell give K_β lines. Higher the atomic number of the target metal, shorter the wavelength of lines.

Normally in X-Ray diffraction, K_α lines are selected and K_β lines are filtered out by using a filter anode of thin foil of the element of atomic number (Z-1) adjacent to that target metal, Z. Other types of mono-chromater especially single crystal are also used. The German physicist Von Laue in 1912 first determined that X-rays diffract from the periodic arrangement of atoms in a crystal, exactly analogous to the diffraction of visible light from a grating. Based on the work of Von Laue, W. H. and W. L. Bragg showed in 1913 that diffraction from a crystal is described by the equation now known as Bragg's law:

$$n\lambda = 2d \sin\theta$$

Where n is order of the reflection, d is inter-planner spacing, θ is one half of the diffraction angle and λ is wavelength.

When n = 1, the reflections are called first order and when n = 2, the reflections are second order. However, Bragg equation for the second order reflection from a set of planes hkl is $2\lambda = 2d_{hkl}\sin\theta_{hkl}$

Diffraction experiments require X-ray wavelengths of the order of the inter-atomic spacing to produce interference, and hence typical wavelength ranges are 0.07-0.2 nm.

Diffraction measurement in the present work are carried out on the WinXPOW Program Package on STOE & CIE instrument equipped with the Cu K_α source having $\lambda = 0.179$ nm (at SCME, NUST). The measurements were carried out with a voltage of 40 KV, a current of 30 mA and measurement angle 2θ varies from 20-80.

2.6   Particle Size Analysis

Particle size analyzer is an automated device for determination of the particle size distribution. This measurement of particle size distribution is used for fundamental studies and quality control in production processes in many diverse fields such as fine ceramics, cement, pharmaceuticals, metal powders, industrial minerals and ores, explosives, solid fuels, foods, drugs and beauty care emulsions, micelles, polymers, coatings and adhesives, pigments and dyes, carbon black and other minerals, additives and fillers used in rubber, plastic and paper industry etc. etc. Most particle size analyzers use one geometric parameter and make the assumption of a spherical particle shape. The basis for analysis can be any of the obvious geometric values, such as surface area, projected area, maximum dimension, minimum cross-sectional area, or volume. Size data are most useful when presented within the context of the measurement basis and the assumed particle shape.

2.6.1   Particle Size Measuring Techniques

The size of the particle depends on the measurement technique, specific parameter being measured and particle shape. A number of techniques are presently used to determine the particle size of a sample powder. Some of these techniques are microscopy, screening, sedimentation, light scattering, electrical zone sensing, light blocking, and X-ray technique.

2.6.1.1 Microscopy

It is a widely applied technique used for the sizing of particles. Microscopy is reasonably accurate, but the tedium of sizing statistically significant quantities of particle leads to use the automatic image analyzer. The image for analysis is generated by optical, scanning electron, or transmission electron microscopes. The instrument choice depend on the particle size; however in the SEM, the larger depth of field is a distinct advantage, especially since it shows surface topography and provides EDS spectra for compositional analysis. By microscopic counting of diameter, length, height or area a frequency distribution is generated. The distribution records the relative frequency of the selected particle dimension.

Intelligent discrimination between single and multiple particles is a common problem in particle size analysis. Counting two or more small particles as a large particle will skew the distribution towards the coarse sizes. Improper size measurements will give false indications.

2.6.1.2 Screening

Screening is a common technique for rapidly analyzing particle size. A mesh of square grid of evenly spaced wires is used. The mesh size is determined by the number of wires per unit length. The opening sizes varies inversely with the mesh size, large mesh sizes imply small opening sizes and vice versa. This technique is usually applied only to particles larger than 38 μm. There are electroformed meshes available down to 5 μm, but agglomeration and particle adhesion to the mesh are common problems in these meshes.

2.6.1.3   Sedimentation

This technique is mostly applied to smaller sizes. Particles settling in a fluid reach a terminal velocity dependent on both particle size and fluid viscosity. So the particle size can be estimated from the settling velocity. Depending on the particle density and shape, sedimentation techniques are nominally applicable to particles in the 0.02 to 100 μm range. High fluid viscosities are needed for analysis of larger particle sizes. Particle size analysis by sedimentation uses a predetermined settling height and places a dispersed powder at the top of the tube. Measurements of the amount of powder settling at the bottom of the tube (weight or volume) versus settling time then allows calculation of the particle size distribution. The fastest settling particles are the largest while the smallest take considerable time to settle.

2.6.1.4   Light Scattering

In streaming techniques for size analysis, particles are dispersed in a moving fluid. Size determination is based on a discontinuity in the fluid stream due to the presence of the particles. With careful instrument calibration, the discontinuity size can be related to particle size. Streaming methods provide a large dynamic ratio; the ratio of the largest to smallest particles that can be measured simultaneously.

A versatile streaming technique is light scattering. Low angle Fraunhofer light scattering using monochromatic (LASER) light and dispersed particles is widely used for automatic particle size distribution. Particle size affects both the intensity and angular extent of scattering. A fluid stream with dispersed particles is passed in front of a detector system. The data related to particle size are collected using a photodiode detector array. With coherent (Laser) light the angle of scattering varies inversely with the particle

diameter. Computer analysis of the intensity versus angle data determines the particle size distribution. The particle size range is 1 to 200 μm.

In our experiments, the laser scattering particle size distribution analyzer HORIBA LA-920 was used for determination of the glass powder particle size distribution. On this instrument, particle sizes ranging from 0.02 to 200 microns are divided into 85 sectors and the full range is measured at one time with no adjustment. A measurement time of 20 seconds is usually sufficient.

CHAPTER 3

EXPERIMENTS, RESULTS AND DISCUSSION

Cold rolled, fine grained, annealed Kovar alloy was used in this investigation. The chemical composition of the Kovar alloy (ASTM, F15) is reported as (in wt %):

Table 3.1: Reported chemical composition of the as received Kovar alloy (ASTM, F15)

Fe	Ni	Co	Mn	Si	Ti	Cu	Al	Mo	Zr	C
53.47	28.85	17.15	0.17	0.15	0.03	0.03	0.012	<0.01	<0.01	<0.01

The borosilicate glass powders used in this study were commercially available (China grade) Chine DM305 and G350. The nominal composition was reported by the manufacturer as (in wt %)

Table 3.2: Reported composition of both types of glass powder, show a slight variation in their composition.

Glass Type	SiO_2	B_2O_3	Na_2O	Al_2O_3	K_2O
DM305	67.5	20.3	3.8	3.5	4.9
G350	70.2	19	8.1	2.4	0.09

The compositions were also confirmed by Geo Science Laboratory Islamabad.

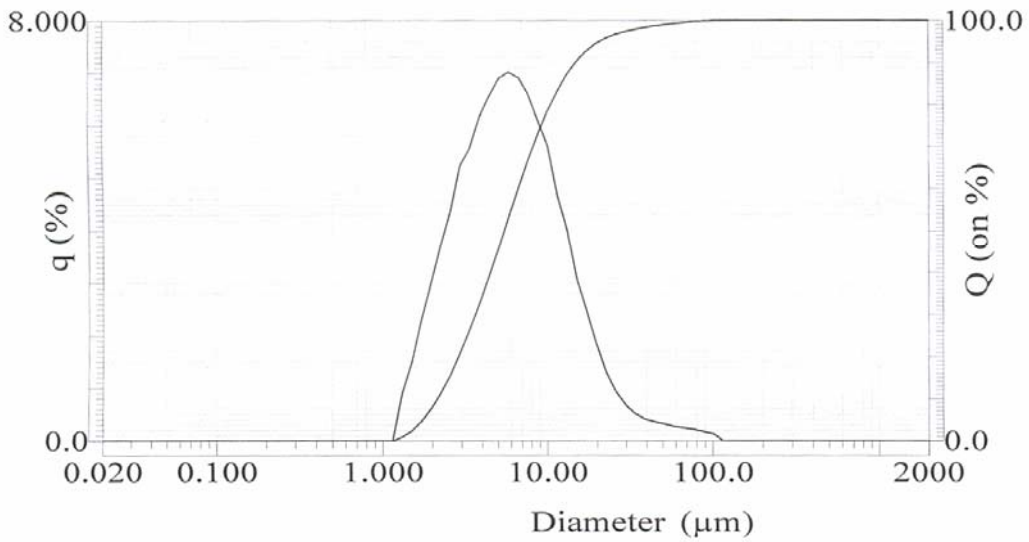The true density of the glass powders were measured by Gas Pycno-meter and recorded as 2.301 g/cc and 2.309 g/cc for glass DM305 and G350 respectively. The particle size analysis was done for the raw and heat treated glass powders by HORIBA LA-920, LASER scattering particle size distribution analyzer at SCME, NUST. To confirm the particle size distribution of the glass powder, SEM of the powder was done

using Scanning Electron Microscope JEOL JSM-6460, using the facility at AWC, operated at 10kv.

The results of the particle size distribution and SEM micrographs are shown below. The distribution of particles on the log-normal curve without any heat-treatment and after heat-treatment is shown in fig 3.1 (a) and (b) respectively. In fig 3.1 (a), the median size corresponding to 50% value on the smooth cumulative particle size distribution is 5.52µm. The mean value shows that almost 88% particles are of 8microns. After heat treating the powder in a muffle furnace at 400°C for a period of 30min and cooling inside the furnace, the results are changed. Agglomeration of the particles takes place. The mean and median both values are changed. In figure 3.1(b), this changing effect is shown. The median size is now 6.24 µm and the mean value now becomes 9.91 thus resulting in denser particles. These results are tabulated in table 3.3.

Table 3.3:   The different parameters of the particles size distribution obtained before and after the heat-treatment of the glass powder

	Distribution of particles of glass powder before Heat-treatment	**Distribution of particles of glass powder after Heat-treatment**
Circulation speed	2	2
Median (µm)	5.52	6.24
Mean (µm)	7.99	9.91
Variance (µm^2)	82.96	146.09
Std dev. (µm)	9.11	12.09

(a)

(b)

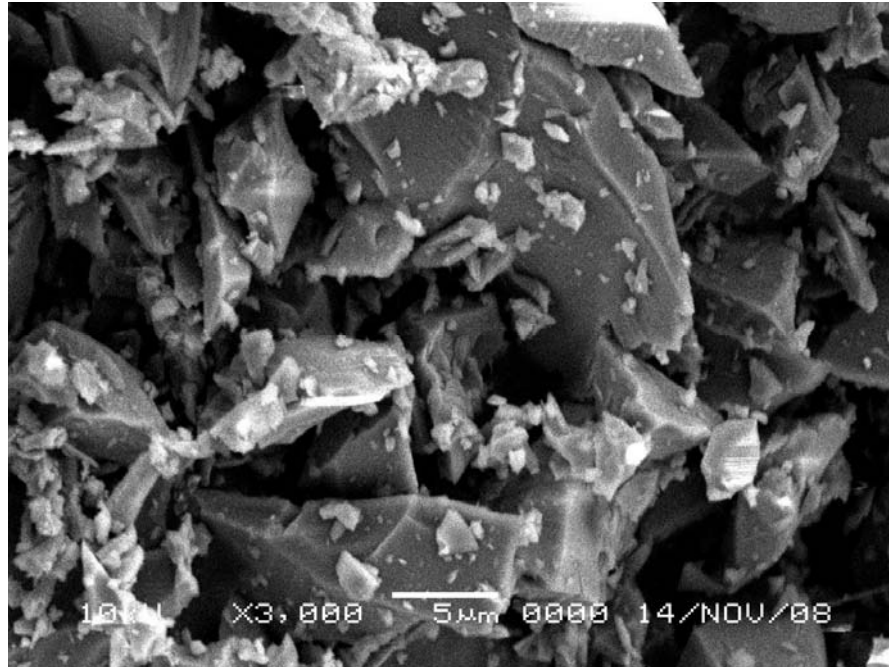**Figure 3.1:** Particle size distribution of raw glass powder DM 305, taken on Horiba LA-920 laser particle size distribution analyzer (a) without any heat treatment, the mean value is 7.99 (µm), (b) after heat treatment of the powder at 400 °C and cooling it in the furnace. Agglomeration results and the mean value become 9.91 (µm)

The results obtained from particles size distribution curves are verified by taking the SEM micrographs of the powder particles. In figure 3.2, some of these micrographs are shown. In fig (3.2a), at a magnification of X3000, it can be clearly seen that most of the particles are 4 to10 μm. a small number is of about 40 to 50 μm. In fig (3.2b), the micrograph at a magnification of X1000 is shown. Agglomeration effects are apparent. Large number of agglomerated particles can be seen.

The thermo gravimetric analysis (TGA), which is used to accurately measure the weight change with temperature and to study the oxidation & decomposition behavoiur of the reaction kinetics, is employed for the study of the behaviour of the metallic glass powder. For the as received glass powder i.e. without heat treatment, more weight loss (approx. 3%) is observed. After heating the powder in a muffle furnace upto 400 °C and keeping it for 30 min in the furnace and then cooling it down to room temperature inside the furnace. The thermo gram shows different behaviour. The weight loss becomes less i.e. now it is approximately 1%. This weight loss may be due to the moisture content present in the powder.

Before making the glass-metal bond, the as-received Kovar wire was cut into pieces (ϕ 0.80 x 10mm, ϕ3 x 10mm) and polished using 600, 300 grit SiC abrasive. The material was then degreased by cleaning sequentially in 10% ammonium hydroxide, 10% nitric acid, de-ionized water and ethanol. Finally, the alloy was pre-oxidized at 750°C for 10 min in flowing air.

(a)
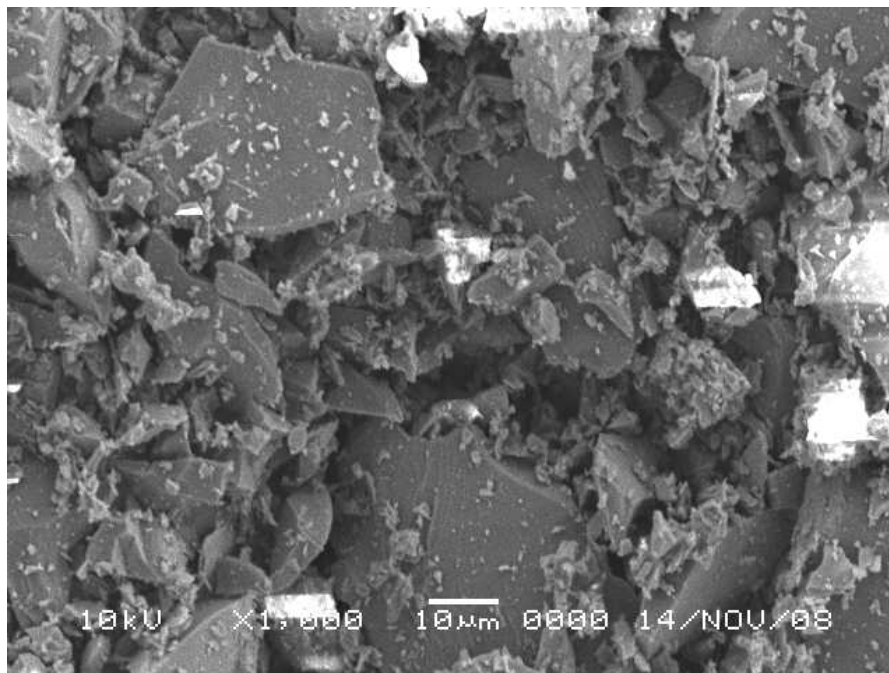
(b)

Figure 3.2: SEM micrographs of the powders showing the particle size distribution. (a) Particles of 4 to 10 μm cover the major area; (b) Agglomeration effects of the particles can be seen.

3.1   Formation of Glass beads

The glass-metal seals were produced by the following procedure. The raw

material and semi-products required for the glass beads are:

Glass powder (DM350 and 305) 100 ± 1 gm, Paraffin wax 2.5 ± 0.25 gm, Oleic Acid 1.5 ±

0.25 ml. The raw material was heated at 150 ± 10 °C in the oven for about 2 hours. After

melting and homogenizing the paraffin with oleic acid, this mixture was added to the

glass powder and ground evenly.

The beads are form by bead forming press at <1 Ton. The photograph of the bead

forming press is shown in figure 3.3 below. The formed beads are kept in SS pan to pre-

sinter them. The pre-sintering is done as per the following order:

Pre-sintering	150 ± 10 ˚C	60 ± 3 min
Paraffin exhaustion	450 ± 10 ˚C	60 ± 3 min
Forming	750 ± 10 ˚C	7~10 min

Figure 3.3: The bead forming press that is used to form the green compact of the bead
before pre-sintering

The final beads formed are inspected visually and are kept with care in sealed containers to avoid damage. The micrographs of the pre-sintered bead in figure 3.4 show clear porosities. But the porosity in the bead has no effect on the final product. As after complete melting, the bead homogenize with the Kovar due to its matching thermal coefficient expansion.
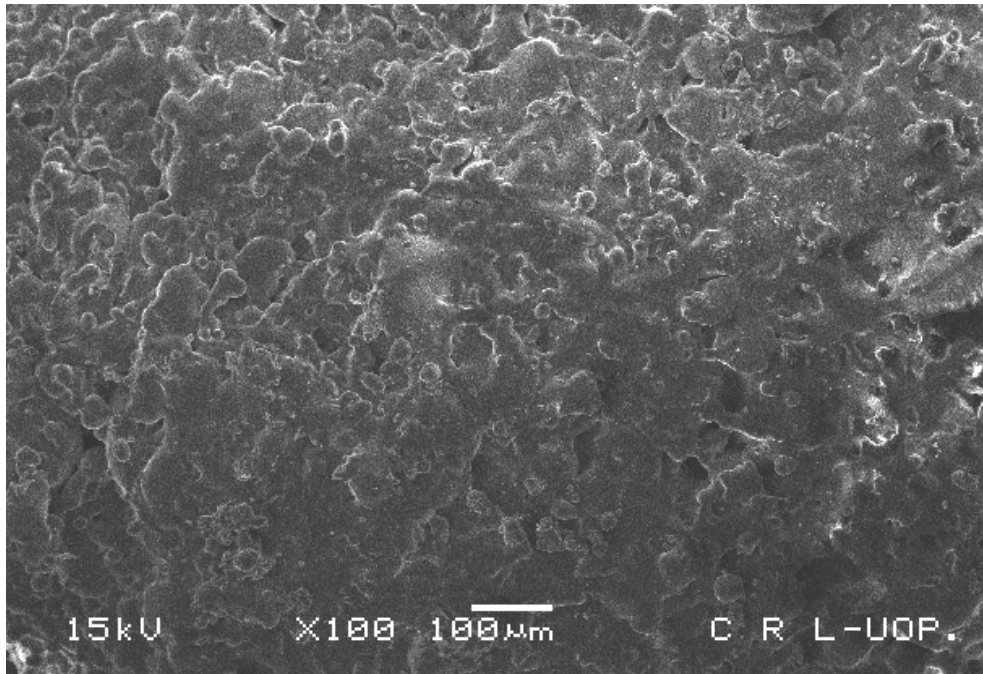
Figure 3.4: SEM micrograph of the pre-sintered glass bead at a Temperature of 750°C taken on the surface at 15kv and X100 magnification showing the good sinter-ability. Pores of various sizes are also apparent.

3.1.1 Sintering of Glass-Metal

At temperature 700 ± 10 °C, the flow of cool water is started into the cooling chamber of the furnace while the transport belt is switch on.

Different process parameters were adopted for the preparation of various samples. All these parameters were set after acquiring the temperature in the sintering furnace at 920 ± 20 °C. N_2 gas was purged for a period of 20 min. The graphite dies (blocks) were placed over the transport belt inside the furnace, allowing them to move over the belt in different

zones of furnace gradually. Glass to metal sealed parts are held at temperature for the specific time and then cooled by directly exposing to

(i)   atmospheric air, and

(ii)   less than 175 °C to avoid excess oxidation and/ or thermal shock which may cause distortion.

The melted glass beads with Kovar lids and rods are checked and analyzed. He-gas test is also performed. The resistance is checked with meggar. The value of the resistance is $\geq$ 500 MΩ.

3.2   Characterization of the Glass-Metal Seal Specimens by SEM

The glass-metal sealed lids with different combinations of glass powder and various process parameters are selected and prepared for the SEM investigation. Using 800, 600, and 300 grit SiC abrasive and 0.1µm alumina paste on diamond polisher cloth, the samples were prepared and polished according to the stub of the SEM machine JEOL, inc. Model No: JSM 5910 at CRL University of Peshawar operated at 10 - 15 kv.

The four different samples prepared at different parameters are as follows:

Sample 1:

N$_2$ gas is allowed to purge at 5m^3/hr and the speed of the transport belt is kept at 3cm/min (i.e. Short time for the glass-to-metal bonding in the furnace and lower N$_2$ environment). Further at the exit from the furnace the sample is suddenly exposed to ambient air. Due to short time to remain inside the furnace, insufficient oxidation is expected which cause a defected bond at the glass-metal interfaces. The oxidation layer of Kovar is mainly composed of iron oxides. It is reported that the pre-oxidized layer is a

mixture of FeO, hematite (Fe_2O_3), magnetite (Fe_3O_4)[23,24] , and a complex zone including

magnetite and an underlying oxide enriched in nickel and cobalt[12]

The micrograph for such a sample is shown below:
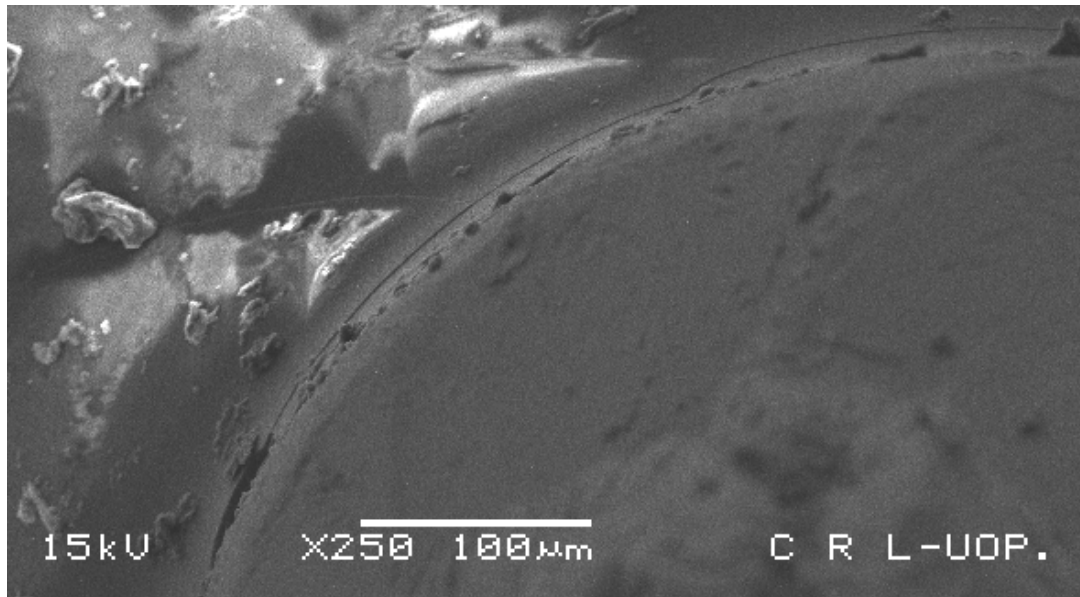
Figure 3.5: SEM Micrograph showing the cracks and de-bonding of the glass–metal at the interface of the seal for the sample 1.

The de-bonding is apparent. Clear cracks can be seen at the interface. The severe thermal

shock that the sample receives at the exit from the furnace may be the root cause for this

de-bonding and cracks.

Another reason is the formation of thickest layer (exceeding 6.5 μm) of oxide on

the alloy surface during pre-oxidation process. This layer must be prevented because this

causes hindrances in the complete diffusion of the melted glass, leaving residue FeO thus

resulting in continuous porous channels formed on the interface between the residue FeO

and the alloy, which cause poor quality defected seal and cause air to leak from the

junction. In the study of McCormick and Zakraysed [25], they found that oxide layer

exceeding 6.5 μm would lead to poor glass-to-metal sealing and proposed that the

optimum thickness of the oxide layer should be 2–6.5 μm. On the other hand, Yext et al.[26] found that better junction quality can be achieved when the thickness of the oxide layer falls within the range of 2–10 μm. In their research, formation of small air bubbles was observed in oxide layers exceeding 20 μm in thickness, which weakened the glass-to-metal junction.

Sample 2

N_2 gas is allowed to purge at 5m³/hr and the speed of the transport belt is kept at 2.5cm/min (i.e. more time for the sample to remain inside the furnace) allowing lower N_2 environment but more time in the furnace for the sealing of glass to metal. Further at the exit from the furnace the sample is again suddenly exposed to atmospheric air. Improvement is observed due to the extra time given to the sample to remain in the furnace. But the temperature gradient at the exit from the furnace is again enhancing the de-bonding and cracks in the glass-metal seals. This case is best understood from the micrograph shown below:
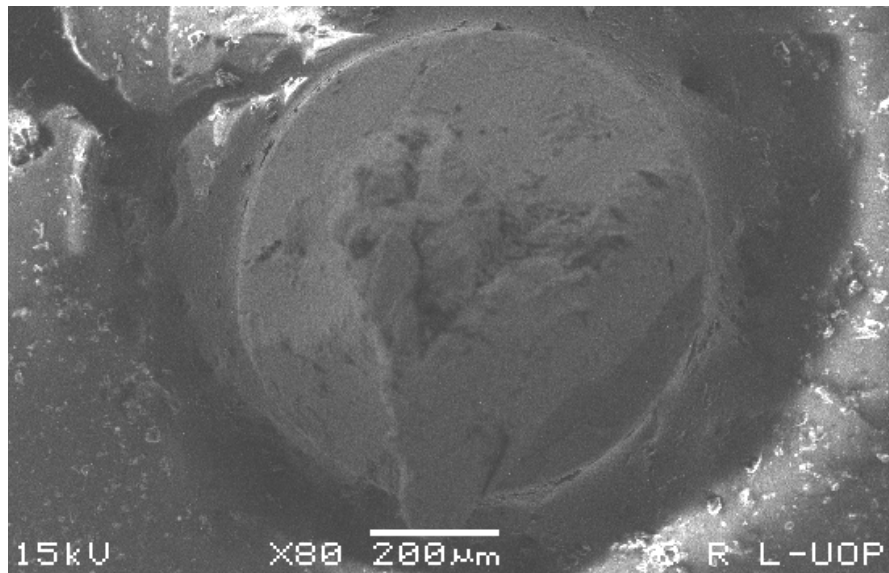
Figure 3.6: SEM micrograph showing the somewhat improved bonding characteristics of the glass to metal seal.

Partial de-bonding can be seen which shows that giving more time to the glass melt to homogenize with the Kovar alloy enhances the good sealing properties. But again the environmental effects influence the glass-metal junction adversely causing a poor bond at the interface.

Sample 3

N$_2$ gas is allowed to purge at 6m^3/hr and the speed of the transport belt is kept at 3cm/min (i.e. more N$_2$ gas environment but less time for the sample to remain in the furnace)

The exit conditions are now changed. The lid remained closed until the product inside the graphite box came to the ambient temperature. The effects of sudden shrinkage and thermal shock are minimized. The samples are no more exposed in the atmosphere suddenly. The graphite blocks are cooled down to room temperature and the samples are then drawn out for further investigation. Good results are obtained by minimizing the thermal shock that the sample receives resulting in low shrinkage thus improving the bond quality at the glass-metal seal interface. Giving a more N$_2$ environment for more time, the seal will become defected and weaker.

Failure occurs entirely in the glass for the nitrogen gas environment samples. Numerous bubbles are formed in the glass and at the interface. The bubbles act to lower the strength of the glass. But Co enrichment increases, which strengthens the bond.

As the good junction and high bonding strength seals require three factors: (i) sufficient thickness of the oxide scale on the pre-oxidized metal surface, (ii) optimum sealing time and temperature for the glass to wet the pre-oxidized alloy, and (iii)

dissolution of the oxide scale into the glass without devitrification to develop matching dilatometric behavior of the interfacial constituents.

SEM micrographs for this case are shown below:
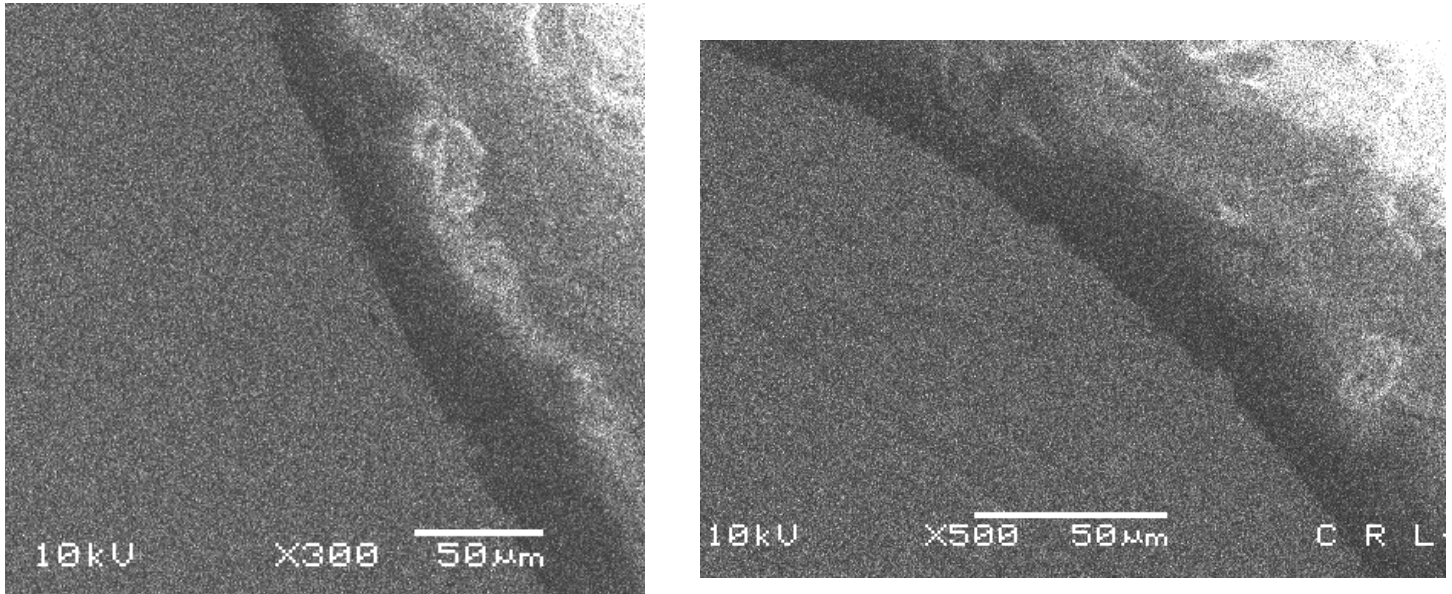
(a)   (b)

Figure 3.7: SEM Micrographs showing the improved sealing behaviour after utilizing the improved process parameters. (a) glass-metal seal interface with outer Kovar disc (b) interface of the seal with inner Kovar wire and glass DM 305

Sample 4

N_2 gas is allowed to purge at $6m^3$/hr and the speed of the transport belt is kept at 2.5cm/min (i.e. more time and more N_2 environment for the sample to remain inside the furnace). This is the optimized case for the sealing of the glass-metal. Best ever results are obtained using these process parameters.

During pre-oxidation, it is possible that the oxide layer advances by diffusion of Fe through the oxide layer toward the surface[27]. This creates open porosity in the alloy in which iron-rich glass penetrates during bonding treatment, so creating a strong physical

adhesion. i.e. the joining is strong in the presence of FeO phase, because its porosity constitutes a low resistance zone.

Zanchetta et al. [28] reported that wustite (FeO) existed as an interlayer in the joint to bridge the difference in bonding between glass and alloy. The existence of the wustite interlayer has been confirmed only in the case of joining under normal atmosphere. The FeO layer formed on the Kovar alloy surface after high-temperature oxidation treatment plays a crucial role in the sealing and joining between the glass and alloy. Its quality will determine the excellence of the glass-to metal junction. Pask[29] suggested that the optimum rate of oxidation should range between 0.3 and 0.7 mg cm^{-2}, while Abendroth [30] reported that better adhesion can be achieved at 0.6–1.1 mg cm^{-2}, and the oxide layer formed should be at least of 2.5 μm thick to ensure better sealing effect and greater bonding strength.

SEM micrograph in the figure 3.8 (c) below, shows the interfaces of the joints bonded under normal atmosphere that can be divided into four regions

Zone I: The bulk of the alloy with no change in the chemical composition.

Zone II: The porous Fe-depleted area. Porosities are present along the alloy surface and the glass is penetrated into these pores. These pores are beneficial for the forming of a good seal unless they become voids. The Fe-enriched glass flows into the pores on the alloy surface forming a mechanical bonding.

Zone III: The Fe-rich zone in the glass which occurs by the dissolution of the iron oxides and Fe diffusion into the glass during joining. The controlled FeO layer that is formed enhances the strength of the seal thus resulting in a good quality glass-metal seal.

Zone IV: The bulk of the glass again with no change in the chemical composition.

The SEM micrographs of the glass-to-metal seals of this type are shown in the figure below.
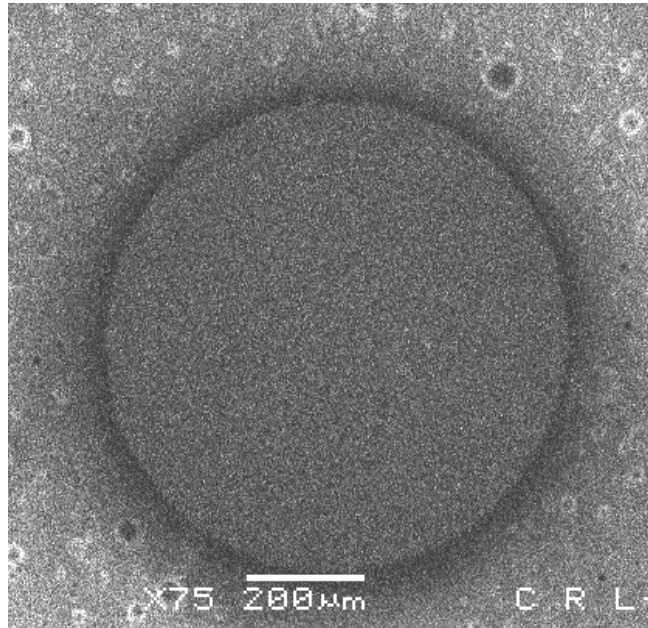
(a)
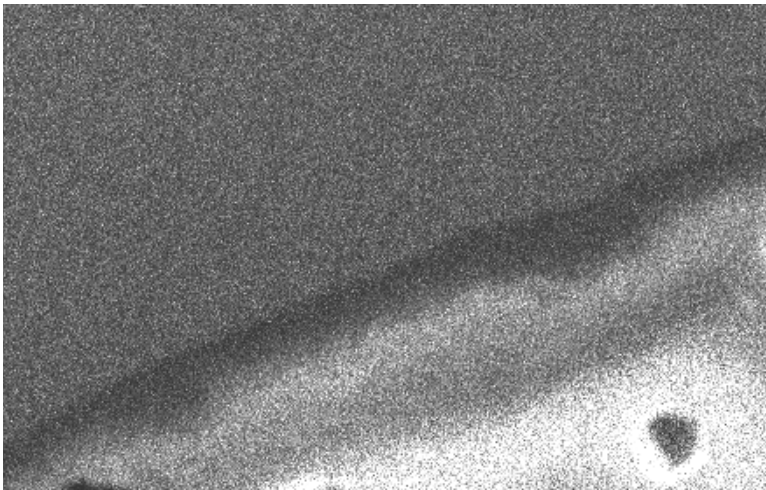
(b)

(c)

Figure 3.8: SEM micrographs of the Interfaces of the seal with Kovar and glass. (a) and (b) show the improved bonding by changing the process parameters. (c) Different zones that form during the glass to Kovar seal.

The thermal expansion coefficient of Kovar alloy is around 5.3×10^{-6} $°C^{-1}$, which is close to that of glass (5.15×10^{-6} $°C^{-1}$); while that of pure FeO is 12.2×10^{-6} $°C^{-1}$. Combinations of glass and FeO of different proportions have different thermal expansion coefficients. Zanchetta and Lefort[24] have reported that the thermal expansion coefficient of 80% glass + 20% FeO was 6.1×10^{-6} $°C^{-1}$; 60% glass + 40% FeO, 7.8×10^{-6} $°C^{-1}$; 40% glass + 60% FeO, 8.4×10^{-6} $°C^{-1}$; Fe-depleted Kovar alloy, 10.2×10^{-6} $°C^{-1}$. The t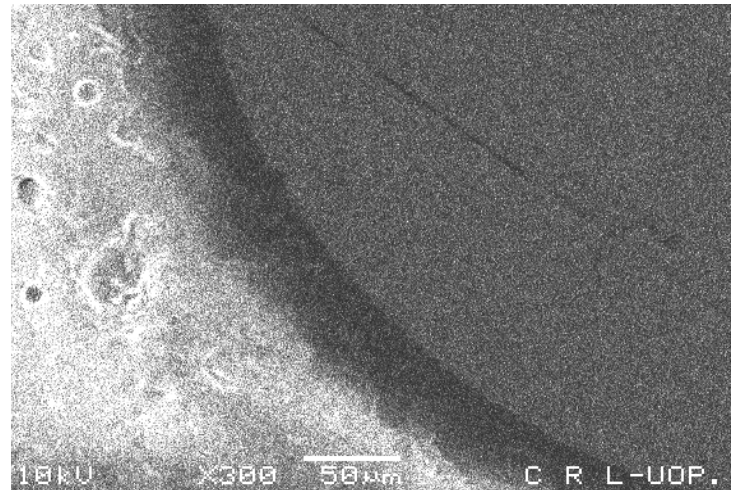hermal expansion coefficient becomes higher with increasing content of FeO, with the exception of the Fe-depleted Kovar alloy. In spite of its lower Fe content, the Fe-depleted Kovar alloy has a high thermal expansion coefficient two times that of Kovar alloy and closes that of pure FeO. This transforms the elements in the Fe-depleted zone in the Kovar alloy. To achieve good joining effect requires a buffer zone with appropriate thermal expansion coefficient. In this study, the Fe-rich glass forms a buffer zone with thermal expansion coefficient close to that of the underlying alloy. However, incomplete dissolution of FeO will lead to mismatched thermal expansion coefficients between glass and alloy, and cracks will easily form during cooling. In other words, there should be sufficient time for FeO to react with glass and dissolve entirely in order to achieve good sealing. Moreover, pre-oxidization treatment of Kovar alloy can enhance the wettability of glass. Fe-depleted zone formed during oxidation is of great porosity, which favors the penetration of glass into the open pores, thus enhancing the mechanical adhesion of glass on the alloy surface.

These results are in agreement with those presented by C. Chanmuang[31] et al. The micrograph is shown below in fig 3.9. The four different zones can clearly be seen. The Fe-rich zone in the glass (the region III) yields good thermal expansion matching. The Fe diffusion distance extends to about 60 μm in the joint bonded under normal atmosphere.

A dendritic phase is observed within the Fe-enriched zone in the glass adjacent to the interface. This dendritic phase extended about 10 μm into the glass.
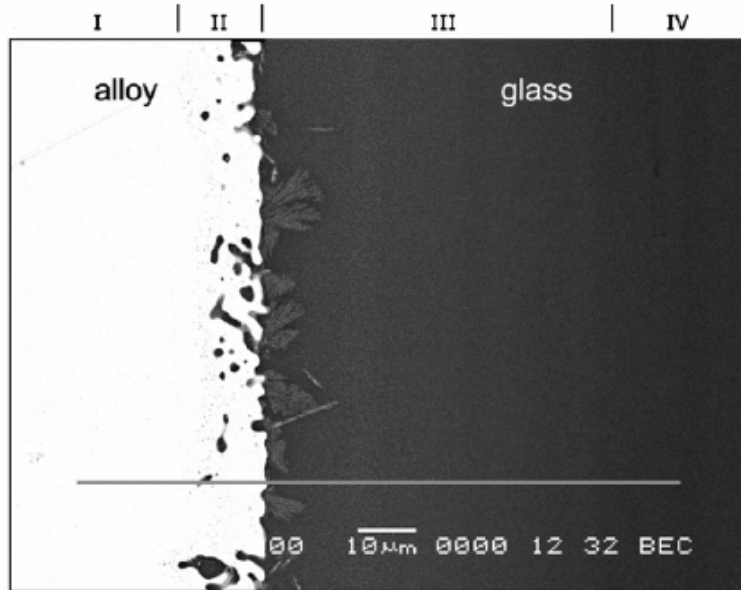
Figure 3.9: SEM micrograph of the cross section of the joint formed under normal atmosphere. (C. Chanmuang et al[31])

The duration of the bonding thermal treatment is very important and its role is well summarized in Fig. 3.10 which presents diagrams describing the thermal expansion coefficients (CTE) evolution in the interfacial zone according to the time of thermal treatment.

If it is too short Fig. 3.10 (a), the brittle oxide layer remains and the FeO-dissolved gradient is very strong, so that the bonding is weak. If the treatment duration corresponds to that of a complete reaction or dissolution of the FeO layer in the glass Fig. 3.10 (b), it is the best case where there is a large gradient of FeO in the glass, hence a good fitting of the thermal expansion coefficients in the interfacial zone, and a sufficient penetration of the glass in the superficial porosity of the alloy. For too long times Fig. 3.10 (c) homogenization of the glass leads to a significant gap of the thermal expansion

coefficients at the glass to alloy interface and the bonding breaks during cooling at the end of thermal treatment.
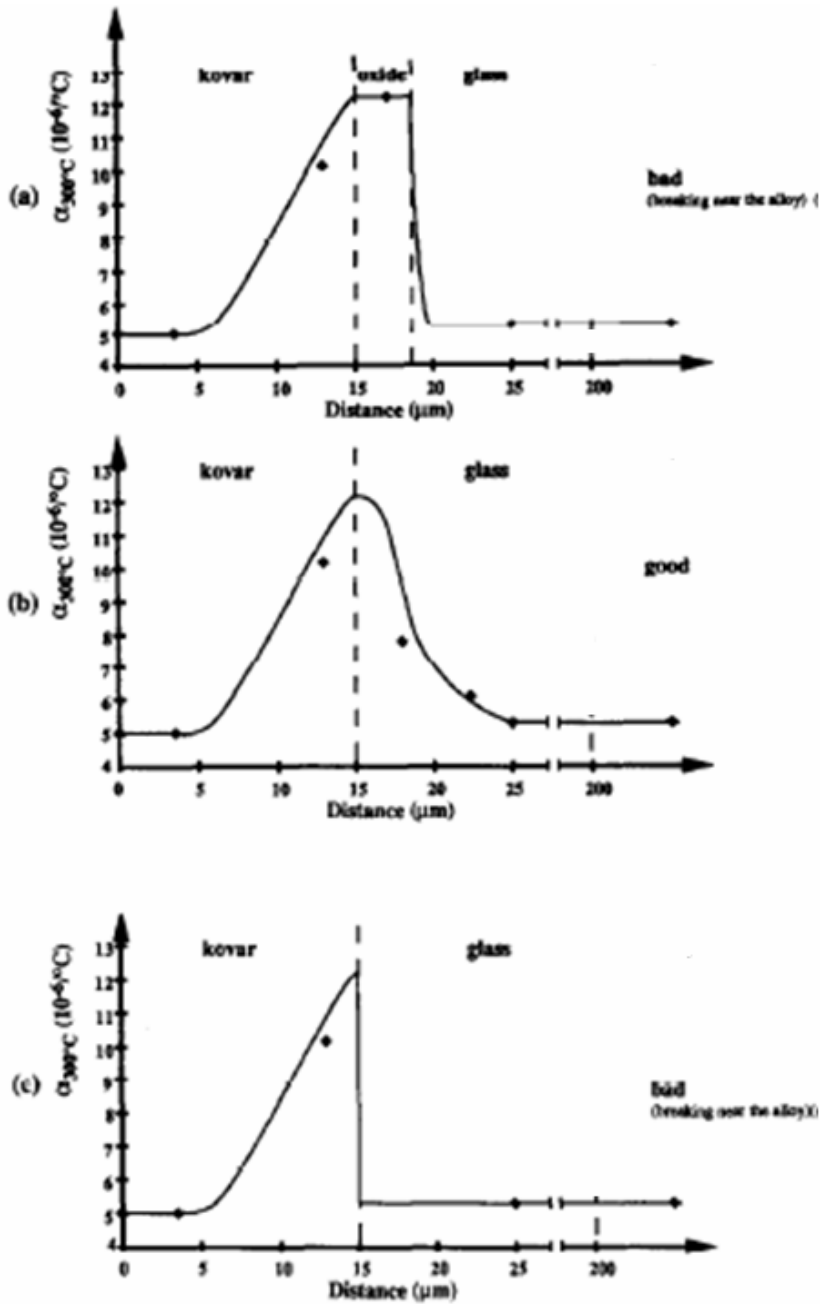
Figure 3.10: Dilatometric profile of the interfacial zone: (a) oxide layer slightly dissolved; (b) oxide layer almost totally dissolved; (c) the whole oxide layer is dissolved.

Results of this study show that at 900°C - 925°C, FeO on the interface react completely with glass. Further increase in thermal treatment temperature will accelerate the diffusion of dissolved FeO into the glass. As shown in the figure 3.11, the Fe in the glass zone near the interface appears unsaturated with FeO and metal bonding[32]. Thus, the optimum temperature may range between 900°C and 950°C. Within this thermal temperature range, Fe in the glass can spread to an appropriate distance, forming a wider reaction layer, and FeO can be entirely dissolved in the glass. Glass saturated with FeO can in turn enhance the glass-to-alloy bonding. In addition, adjusting the concentration gradient of the elements in the zones neighboring the interface can ensure matching thermal expansion coefficients in adjacent zones, thus preventing the formation of cracks during cooling and processing
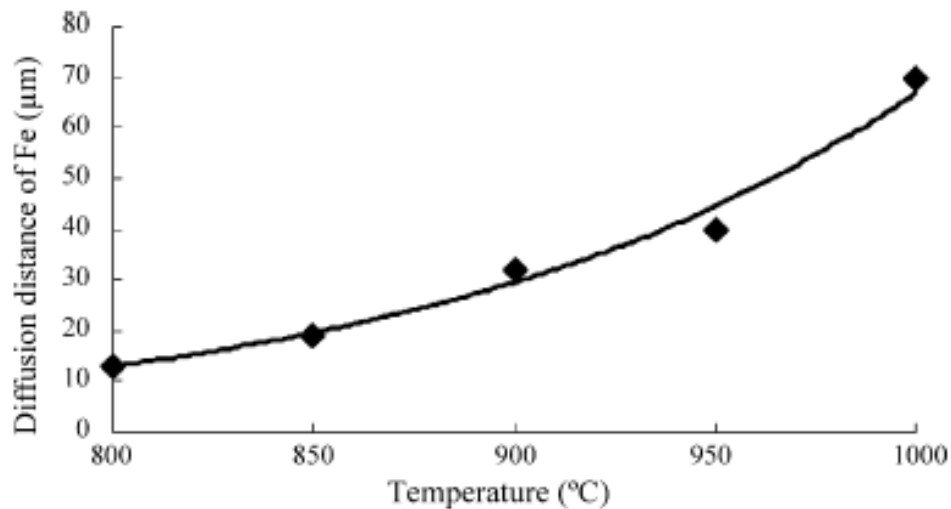
Figure 3.11: Relationship between diffusion distance and temperature of Fe in Glass (T.-*S. Chern, H.-L. Tsai / Materials Chemistry and Physics* **104** *(2007) 472–478)*

3.3   Leak / Failure Tests

The most common method of detecting failure is to subject the component to a Helium/ Argon leak check. Helium, Argon and die penetrate leak tests were employed to the glass-metal seals. The sample 1 showed leakage from all around within a few minutes during the die penetrate test. The sample 2 shows somewhat better results but still leakage is observed. The sample 3 and sample 4, having improved process parameters show good results. No such kind of leakage was observed.

Figure 3.12: The defected vs. un-defected glass-metal seal using the die-penetrate leak test method

In Ar gas test, the samples were placed in sealed container and it was filled with Ar gas. If the seal is defected, i.e. some cracks are present, a stage comes where the gas leaks out and no pressure is sustained in the container.

In Helium gas test, typical standards for hermeticity range from 10^{-6} to 10^{-8} cm^3/s He (standard temperature and pressure). Hermeticity can be lost either by separation at the glass-metal interface or by glass fracture. Failure may also depend upon other factors

such as seal size, surface flaws in the metal or glass, internal flaws in the glass, or slow crack growth. Too much stresses on glass are also susceptible to fracture by subsequent processing and handling, such as when leads are attached to pins.

In a glass-metal seal some stress is usually present owing to a differential contraction between the members of the seal that takes place during cooling of the seal. At high temperatures, stress in glass can be dissipated by viscous flow. Thus the stresses are reduced to a very low value during the annealing process. During cooling from the annealing temperature, a stress will be developed if there is any difference in the rate of contraction of glass and metal. This will usually occur even for a glass-metal combination that shows low stress at room temperature because of the difference in shape of the glass and metal contraction curves. An appreciable fraction of the stress produced by the initial differential cooling will be lost by viscous flow. As cooling proceeds, a larger fraction of the stress is retained. The stress at room temperature will obviously correspond to cooling through a smaller temperature interval without stress release by viscous flow. The temperature from which cooling without viscous flow would produce the same stress is called the equivalent setting point

The stress is directly proportional to the differential contraction. The proportionality factor is a function of *(a)* the stress direction, *(b)* the position in the seal where the stress is measured, (c) the seal dimensions, and *(d)* the elastic constants of glass and metal

The most notable analyses of this kind are those of Hull and Burger[33] and of Poritsky[34] for the cylindrical seal [35,36,37]. Such analyses may not yield a complete description of the stress in an actual seal because during cooling of the seal after the

annealing treatment, a certain amount of viscous flow takes place in the glass which may not be the same in all directions.

The best experimental analysis of stresses in cylindrical seals is that of Redston and Stanworth [38,39]. In addition to the axial stress, they have also measured the radial and tangential stresses. Their results are not in accord with the simple theory of beaded wire seals but check very well when the effects of viscous flow during cooling from the annealing temperature are considered.

CHAPTER 4
CONCLUSION

Kovar alloy undergoing pre-oxidation treatment in furnace heated at 700°C for 10 min under flowing nitrogen gas would obtain good wettability. Although nitrogen in access results in defected bonds having cracks in it but as reported the Co present in the Kovar alloy enriches in this environment thus resulting in the strengthening of the bond. This suggests that Kovar alloys formed successful glass-metal bonds, not just because of the excellent thermal expansion matching, but also due to preferential diffusion of cobalt to the oxide surface. Therefore, it was observed the in glass-seal applications, N_2 environment is necessary to form cobalt oxide that improves the hermeticity of the bond in addition to the strong FeO layer at the interface.

Four different process parameters were adopted. It was observed that keeping the belt speed at 3cm/min that results in a short period of time for the sample to remain inside the furnace, allowing N_2 gas to purge at 5m^3/hr, and suddenly exposing the glass-metal seal formed to ambient temperature, due to insufficient oxide inter-layer, and sudden thermal shock, defected bond having cracks is obtained. Some improvements are achieved when the process parameters were changed. By giving optimum process parameters i.e. purging N_2 gas at 6m^3/hr (for cobalt enrichment), lesser belt speed at 2.5cm/min thus giving more time for the formation of the bond, and avoiding the sudden thermal shock received by the glass-metal seal, a strong defect-free glass-metal seal is achieved. Thus for the bond obtained, the interface can be described into four zones, namely Kovar alloy (base material) zone, Fe-depleted Kovar-alloy zone, Fe-rich Kovar-alloy area, and glass bulk area. The oxide layer of Kovar alloy obtained at high-

temperature oxidization treatment is composed mainly of FeO. The layer closest to the underlying alloy is iron depleted but Co-rich and with great porosity. This Co acts as porosity generators which is beneficial in a strong bond. Reaction between glass and Kovar alloy leads to the dissolution of Kovar alloy in the glass. Not only can this enhance the quality of the wet surface, but also achieve good sealing and joining.

4.1 Future Suggestions

Some suggestions are given below for future study.

1 Glasses of various combinations like Corning 7052, 7056, borosilicate glass etc. can be used for glass-Kovar seal applications

2 Pre-oxidation of Kovar alloy at different temperatures may be performed to compare the bond strength due to the FeO interlayer.

3 The behaviour of various process parameters i.e. different temperatures, belt speeds etc. applied to the glass-metal seal inside the furnace can be studied.

4 Electron spectroscopy for Chemical Analysis (ESCA) study can be made to completely characterize the composition of the fractured surfaces.

5 Various combinations of metal alloys can be used, and their comparative effects on the glass-metal seals can be studied.

REFERENCES

1   Lithium Battery Technology, Edited by H.V. Venkatasetty, John Wiley & Sons, New York, N.Y., 1984
[a] Gabano, J.P., Lithium Batteries, Academic Press, Inc., New Yo rk, N.Y., 1983.

2   W.J. Taylor, Anoka, Douglas J. Weiss, Plymouth, Taylor et al., US Patent # 5,306581, Apr. 26, 1994

3   J.A. Pask, From technology to the science of glass/metal and ceramic/metal sealing, Ceram. Bull. **66** (11)   (1987) 1587–1592.

4   B.W. King, H.P. Tripp,W.H. Duckworth, Nature of adherence of porcelain enamels to metals, J. Am. Ceram. Soc. **42** (11) (1959) 504–525.

5   J.A. Pask, New techniques in glass-to-metal sealing, Proc. IRE **36** (1948) 286–289.

6   G.Wallis, D.I. Pomerantz, Field-assisted glass–metal sealing, J. Appl. Phys. **40** (1969) 3946–3949.

7   G. Wallis, Direct-current polarization during field-assisted glass–metal sealing, J. Am. Ceram. Soc. **53** (1970) 563–567

8   P.R. Sharps, A.P. Tomsia, J.A. Pask, Wetting and spreading in the Cu–Ag system, Acta Metall. **29** (1981) 855–865.

9   W.F. Yext, B.J. Shook,W.S. Katzenberger, R.C. Michalek, Improved glass-to-metal sealing through furnace atmosphere composition control, IEEE Transactions on Components, Hybrids, and Manufacturing Technology, CHMT **6 (4)** (1983) 455–459.

10   W.H. Kohl, Materials and Techniques for Electron Tubes (Reinhold. 1960) pp. 448-459

11   A. Zanchetta, P. Lefort, Thermal expansion and adhesion of ceramic to metal sealings: case of porcelain—Kovar junctions, J. Eur. Ceram. Soc. **15** (1995) 233–238.

12   A. Zanchetta, P. Lortholary, P. Lefort, Ceramic to metal sealings: interfacial reactions mechanism in a porcelain—Kovar junction, J. Alloys Compd. **228** (1995) 86–95.

13   B. Dunn, Field-assisted bonding of beta-alumina to metals, J. Am. Ceram. Soc. **62** (1979) 545–547.

14   T.R. Anthony, Anodic bonding of imperfect surfaces, J. Appl. Phys. **54** (1983) 2419–2428.

15   R.B. Adams, J.A. Pask, Fundamentals of glass-to-metal bonding: VII, wettability of iron by molten sodium silicate containing iron oxide, J. Am. Ceram. Soc. **44** (1961) 430–433.

16   J.A. Pask, R.M. Fulrath, Fundamentals of glass-to-metal bonding: VIII, nature of wetting and adherence, J. Am. Ceram. Soc. **45** (12) (1962) 592–596.

17   W.B. Thomas, Matched glass-to-metal seal improvements by controlled atmosphere metal oxidation, Solid State Technol. (1986) 73–75

18   R.S.Chambers, Frank P. Gerstle Jr., and S.L.Monroe, "Viscoelstic Effects in a Phosphate Glass-Metal Seal", J. Am. Ceram. Soc.,**72** (6) 929-32 (1989).

19   Leedeke, C.J., Levy, S.C., Crafts, C.C., "Glass-to-Metal Seal Corrosion in Lithium-Sulfur Dioxide Cells" Power Sources **8** (1981), edited by J. Thompson

20   Marincic, N., "High Energy Batteries," Chapter 9 in Lithium: Current Applications in Science, Medicine, and Technology, John Wiley & Sons, New York, N.Y., 1987.

21   Newbury, D. E.; Yakowitz, H.; *Practical Scanning Electron Microscopy*, (S. I. Goldstein and H.   Yakowitz, eds.), Plenum Press **1975**

22   Koshikawa, T.; Shimizu, R.; *J. Phys. D*: *Appl. Phys.*, 1974, **7**, 1303

23   Y. Ikeda,Y. Sameshima, The Seventh Japan Congress on Testing Materialsnon-Metallic Materials, 1964, pp. 127–132.

24   A. Zanchetta, P. Lortholary, P. Lefort, J. Alloys Comp. **228** (1995) 86–95.

25   J. McCormick, L. Zakraysek, A metallographic test for glass-to-metal seal quality, in: Presented at the 1974 International Reliability Physics Symposium, San Francisco, CA, April 1974, p. 24.

26   W.F. Yext, B.J. Shook,W.S. Katzenberger, R.C. Michalek, Improved glass-to-metal sealing through furnace atmosphere composition control, IEEE Transactions on Components, Hybrids, and Manufacturing Technology, CHMT **6 (4)** (1983) 455–459.

27   N. Bicks, G.H. Meier, Introduction to High Temperature Oxidation of Metals, Edward Arnold, London, 1983.

28   A. Zanchetta, P. Lafort, E. Gabbay, Eur. Ceram. Soc. **15** (233) (1995) 233-238

29   J.A. Pask, New techniques in glass-to-metal sealing, Proc. IRE **36** (1948) 286–289

30   R.P. Abendroth, Oxide formation and adherence on an iron–cobalt–nickel glass sealing alloy, Mater. Res. Stand. (September) (1965) 459.

31   C. Chanmuang , M. Naksata , T. Chairuangsri , H. Jain , C. E. Lyman , Mat. Sci. and Eng. A 474 (2008) 218-224

32   T.-*S. Chern, H.-L. Tsai / Materials Chemistry and Physics* **104** *(2007) 472–478 Physics,*

33   A. W. Hull and E. E. Burger, "Glass-to-Metal Seals," *Physics,* **5** (12) 384-405 (1934); *Ceram. Abstracts,* **14** (6) 136 (1935)

34   Hillel Poritsky, "Analysis of Thermal Stresses in Sealed Cylinders and Effect of Viscous Flow During Anneal," *Physics,* **5** (12) 406-11 (1934).

35   H. Rawson, "Theory of Stresses in Two-Component Glass-to-Metal Tube Seals," *J. Sci. Instruments,* **26**, 25-27 (1949) ; *Ceram. Abstracts,* **1950,** April, p. *69a.* This paper deals with the more general case where the inner metal may be a hollow tube.

36   A. W. Hull, "Stresses in Cylindrical Glass-Metal Seals with Glass Inside," *J. Applied Phys.,* **17** (S) 685-87 (1946); *Ceram. Abstracts,*1947, Nov., p. 223a**.** This paper deals with the internal cylindrical seal where the glass is surrounded by a tubular sheath of metal.

37   *G.* D. Redston and **J. E.** Stanworth, "Glass-to-Metal Seals," *J. Soc. Glass Technol.,* **29** (132) 48-76T (1945); *Ceram*
38   Redston and Stanworth, ***op. cit.***

39   G. D. Redston and J. E. Stanworth, "Stresses in Glass-to-Metal Bead Seals at Room Temperature," *J. SOCG. lass Technol.,***30** 11391 201-16T (1946); *Ceram. Abstracts,* 1948, Jan., p. 9f